Nonlinear theory of wetting on deformable substrates

Julien Dervaux, Matthieu Roche, Laurent Limat

Journal Name

ARTICLE TYPE

Cite this: DOI: 00.0000/xxxxxxxxxx

Nonlinear theory of wetting on deformable substrates

Julien Dervaux,*[a] Matthieu Roché,[a] and Laurent Limat[a]

Received Date
Accepted Date

DOI: 00.0000/xxxxxxxxxx

The spreading of a liquid over a solid material is a key process in a wide range of applications. While this phenomenon is well understood when the solid is undeformable, its "soft" counterpart is still ill-understood and no consensus has been reached with regards to the physical mechanisms ruling the spreading of liquid drops over soft deformable materials. In this work we provide a theoretical framework, based on the nonlinear theory of discontinuities, to describe the behavior of a triple line on a soft material. We show that the contact line motion is opposed both by nonlinear localized capillary and visco-elastic forces. We give an explicit analytic formula relating the dynamic contact angle of a moving drop with its velocity for arbitrary rheology. We then specialize this formula to the experimentally relevant case of elastomers with Chasset-Thirion (power-law) type of rheologies. The theoretical prediction are in very good agreement with experimental data, without any adjustable parameters. We then show that the nonlinear force balance presented in this work can also be used to recover classical models of wetting. Finally we provide predictions for the dynamic behavior of the yet largely unexplored case of a viscous drop spreading over a soft visco-elastic material and predict the emergence of a new form of apparent hysteresis. .

1 Introduction

Interfaces between media, whether solid, liquid or gaseous, play a fundamental role over a large range of scales around us. Their physics and physico-chemistry are at play behind phenomena such as self-assembly and protein folding[1,2], adhesion and wetting[3–9], fracture[10] and friction[11,12]. A countless amount of applications relies on the understanding and the control of interfaces (see for example refs[13–20] and references therein). As a consequence, the study of interfaces is of crucial importance to the advancement of our understanding of fundamental bricks of the world and to the development of innovative applications.

In this paper, we will focus on the wetting of solids by liquids. This seemingly mundane phenomenon, the consequences of which we can observe when raindrops hit the windshield when riding a car, offers a wonderful window into the microscopic world. Its most general description requires an understanding of intermolecular forces and capillarity, hydrodynamics, solid mechanics and transport phenomena and it is relevant to a myriad of practical and natural situations[21–29]. Wetting has fascinated scientists for the last 200 years, starting with the pioneering work of Young[30] and Laplace[31] on capillarity.

Thomas Young was the first to understand that the shape of a droplet sitting at the surface of a non-deformable solid depends on the balance between the surface energies associated with the interfaces between the droplet, the solid and the surrounding atmosphere. The angle $\theta_{\rm eq}$ between the solid-liquid interface and the liquid-atmosphere interface measured inside the droplet at the line of contact of the three phases, the triple-phase contact line, is related to the surface energies $\Upsilon_{s\ell}$, Υ_{sv} and $\Upsilon_{\ell v}$ (where ℓ, s and v stand for liquid, solid and vapor) by the Young-Dupré relation (as Athanase Dupré and his son Paul formalized mathematically Young's ideas[32]):

$$\cos(\theta_{\rm eq}) = \frac{\Upsilon_{sv} - \Upsilon_{s\ell}}{\Upsilon_{\ell v}} \tag{1}$$

Two comments should accompany Eq. (1). First, molecules in a fluid flow under stress or strain. Then the surface energy $\Upsilon_{\ell v}$ is equal to the surface tension $\gamma_{\ell v}$ of the liquid[33]. Second, this balance is obtained by neglecting what happens in the direction normal to the surface of the solid.

To the best of our knowledge, Jacob Bikerman was the first to express concerns about the validity of the Young-Dupré model because of the absence of a a surface-normal balance. He reported that a bar of gelatin dipped into a bath of mercury deforms along the contact line in the direction normal to the surface. The amplitude of the deformation is of the order of several tens of micrometers. He argued that this observation invalidates the classical theory of wetting[34,35].

Bikerman's claim initiated a vivid debate in the community. Its closure led to the identification of a length scale intrinsic to the solid-liquid-fluid system of interest that compares capillary forces to bulk elastic stresses, the elastocapillary length ℓ, initially thought to be proportional to the ratio $\gamma_{\ell v}/E$, with E the Young modulus of the compliant substrate[36]. Note that ℓ should not be confused with the elastocapillary length involved in the description of thin elastic plates bending under capillary forces in capillary origamis for example[37,38]. Lester[36] noted that common values of surface tension span the range 10-100 $\mathrm{mN\,m^{-1}}$, leading to $10^{-11} \leq \ell \leq 10^{-5}$ m when E decreases from

[a] Laboratoire Matière et Systèmes Complexes, CNRS UMR 7057, Université de Paris, Université Paris Diderot, 10 Rue A. Domon et L. Duquet, F-75013 Paris, France E-mail: julien.dervaux@univ-paris-diderot.fr

1 GPa (glass) to 1 kPa (elastomer). He argued that the Young-Dupré equation is an excellent approximation to compute the equilibrium contact angle when the substrate has a large Young modulus. This approximation fails when the solid is soft, as a wedge-like deformation known as the ridge forms under the action of capillary forces on the solid (Fig. 1).

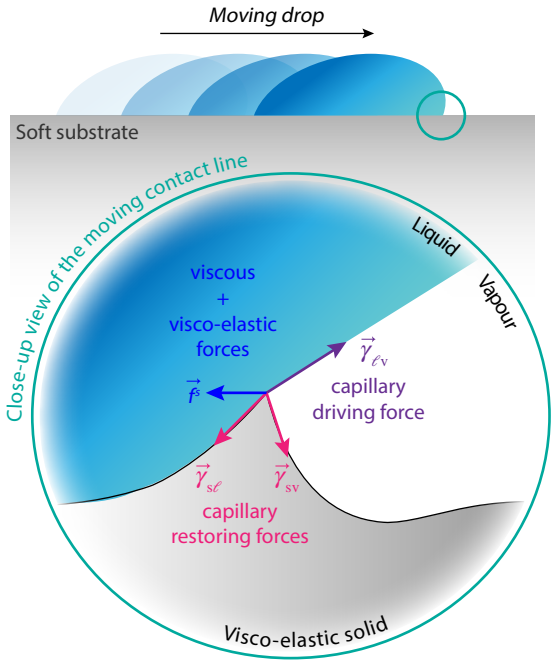

Fig. 1 Schematic representation of the contact line region during the spreading of a liquid on a deformable substrate. The contact line moves at constant velocity. At the contact line, the solid is deformed by the vertical component of the liquid surface tension $\vec{\gamma}_{\ell v}$ and develops a characteristic ridge. The motion of the contact line is opposed both by the visco-elastic force $\vec{f}^{s}$ and by restoring capillary forces $\vec{\gamma}_{sv}$ and $\vec{\gamma}_{s\ell}$ associated with the solid-vapor and solid-liquid interfaces.

The formation of the ridge and its properties are only part of the implications of deformability of the solid for wetting. Droplets in contact with compliant solids such as gels and elastomers move at a pace whose magnitude is set by the viscoelastic properties of the substrate: this effect is known as viscoelastic braking[39–46]. Models of the spreading of liquids on elastomers and polymer brushes based on linear viscoelasticity were proposed[47,48]. These papers highlighted the need to account for the surface energy of the solid Υ_s. The authors were also the first to highlight the importance of the intrinsic elasto-capillary length of the solid, $\ell_s = \Upsilon_s/\mu_0$, where μ_0 is the shear modulus of the solid. Note that Long and his collaborators assume $\Upsilon_s = \gamma_s$, a crucial assumption as we will see later. Then, if x is the distance to the contact line measured parallel to the solid surface, deformations of the solid for $x << \ell_s$ are dominated by capillarity while elasticity dominates for $x >> \ell_s$. Long *et al.*'s remark about the importance of accounting for the surface tension of the solid in problems involving the free surface of a compliant material is now supported by many experiments that illustrate the importance of solid capillarity in various contexts[49–58]. The validity of these models has remained untested against experiments until recently[59,60].

Further progress in the understanding of wetting of deformable solids, *i.e.* elastowetting, had to wait for the widespread availability of new microscopy techniques (confocal, X-ray,...). CarrÃľ and Shanahan reported the first visualization of the ridge using interferometric techniques[44] and could test theoretical predictions of the shape of the ridge available at the time[36,61]. Ten years later, the advent of confocal and X-ray microscopies renewed the interest of the scientific community in the problem. In particular, the ridge could be studied with unprecedented spatial resolution, well below ℓ_s, offering the opportunity to quantify the shape of the ridge close to the contact line and to investigate the capillary-dominated domain[52,62,63].

These studies and many others[64–70] hinted at a possible failure of the elastowetting models proposed up to then. Many of these experiments resort to poly(dimethyl siloxane) (PDMS) elastomers and gels as the compliant solid. These materials are obtained from commercial kits made of two polymeric liquids that contain the reactants to crosslink PDMS chains and form an apparent solid after heat curing. Their surface energy is expected to be identical to that of the liquids γ_{PDMS}. However, experiments reported a discrepancy between the expected value and the one measured in experiments[59,66]. Concerns about the assumptions used in the models arose, in particular with respect to linearity.

The need to switch to nonlinear theories to describe elastowetting was noted early on[59,61,71]. Various suggestions for improvement have been proposed since then. For example, the dependence of the surface energy Υ_s of the substrate on deformation akin to the Shuttleworth effect observed in crystalline and glassy solids[38,72–74] has been hypothesized. This idea seems supported by the reported dependence of the opening angle at the tip of the ridge on the deformation applied to the substrate[75]. However, the interpretation of these fascinating measurements relies heavily on a macroscopic model that lacks a connection with a microscopic theory of capillarity relevant to polymeric materials. Besides, recent experiments[76–79], simulations[80,81] and theory[82] have questioned the existence of the Shuttleworth effect in elastomers. First, experimental measurements of the surface energy of elastomers resulting from studies coupling adhesion tests and contact angle characterization as well as some resorting to other techniques obtain a value for γ_s that is close to that of the base liquids[76,78,83–86]. Second, the Shuttleworth effect results from a change in the intermolecular distance between the molecules of a crystalline solid under strain. No such change is expected in the case of polymeric elastomers: their elasticity results from the reduction of the number of configurations accessible to the deformed polymer chains compared to rest, *i.e.* a loss of entropy. The intermolecular distance does not change, as long as the chains remain far from their maximal extension. At the same time elastomers are only apparent solids, as a probe into their molecular dynamics using nuclear magnetic resonance for example shows that monomers along the chains diffuse around their position as if they were in a liquid state[87]. Fluctuating monomers just below the surface can move to replace monomers displaced along the strained surface. We conclude from this rationale that, as long as the chains are far from their full extension, the Shuttleworth effect is expected to be absent in elastomers, *i.e.* the surface energy of elastomers is equal to the surface tension of the base liquids and it should be independent of strain. Recent simulations support this view[80,81]. On the other hand, if a chemical treatment such as oxidation is applied at the free surface of the

elastomer, the formation of a stiff elastic skin can be induced[88].

Another promising route to a description of elastowetting problems is to move the models beyond linear elasticity. This move is actually required as issues arise when injecting experimental parameters into the predictions of linear elastowetting models. For example, the slope of the surface of the elastomer on each side of the ridge is predicted to be (Eq. 3.18 in ref[69]):

$$\zeta' \sim \frac{\gamma_{\ell v} \sin(\theta_{\ell v})}{2\gamma_s}. \tag{2}$$

This prediction is obtained under the assumption that the angle between the air/liquid interface and the direction parallel to the flat surface away from the ridge is $\theta_{\ell v} = \pi/2$ and $\sin(\theta_{\ell v}) = 1$. Linearity implies that the slopes are small compared to 1. Given Eq. (2), this constraint leads to $\gamma_{\ell v}/\gamma_s \ll 1$, a condition never met in experiments. More fundamentally, the solution obtained within the classical theory of linear elasticity also fails at satisfying the compatibility equations (see Appendix A), suggesting that a more general theory, able to describe discontinuities in an otherwise continuous body, should be used. Thus linear models should be abandoned in favor of non-linear descriptions.

Efforts have been made to move in the direction of a nonlinear theory of elastowetting[82,89–91]. We have shown[82] that the shape of static elastocapillary ridges could be described using values of the physical parameters relevant to experiments by the following nonlinear force balance, here generalized to arbitrary surface tensions and including possible external forces:

$$\vec{\gamma}_{\ell v} + \vec{\gamma}_{sv} + \vec{\gamma}_{s\ell} + \vec{f_{ext}} = \vec{f}_s. \tag{3}$$

Here, $\vec{\gamma}_{\ell v}$, $\vec{\gamma}_{sv}$ and $\vec{\gamma}_{s\ell}$ are respectively the liquid-vapor, solid-vapor and solid-liquid capillary forces per unit of length of the contact line, $\vec{f_{ext}}$ represents additional external forces, other than surface tensions and viscoelastic stresses, that might act on the contact line. In this model, the solid surface energy is assumed independent of strain and equal to its surface tension. The force $\vec{f}_s$ appearing on the right hand side of Eq. (3) is the force per unit of length of the contact line exerted by the deformed solid on the triple line:

$$\vec{f}_s = \lim_{\Gamma \to 0} \int_\Gamma \mathbf{T} \vec{n}_\Gamma \mathrm{d}\Gamma \tag{4}$$

where Γ is a contour enclosing the contact line in the deformed configuration, $\mathbf{T}$ is the true (Cauchy) stress (to be defined below) and $\vec{n}_\Gamma$ is the outward unit vector normal to the contour Γ. This relation is nonlinear because both $\mathbf{T}$ and $\vec{n}_\Gamma$ depends on the deformation of the substrate.

Equation (3) is a generalization of the equation that describes equilibrium at the contact line between three immiscible fluids, known as the Neuman construction[4]. This form accounts for the presence of external forces and for the ability of the substrate to sustain shear. The latter is of crucial importance, as there is a discontinuity of the slope (and hence the strain) at the triple line when the solid is compliant enough to form a ridge. The elastocapillary ridge is then a singular structure. A description of this structure in the context of the theory of defects[92–94] shows then that the force $\vec{f}_s$ does not vanish. Moreover, the prediction for the stress field around the ridge indicates that it is similar to the terminal line of a generalized disclination[95] whose strength can take any value between -1/2 and 1/2 as there is no underlying lattice structure, in contrast with disclinations in crystals. Then, a localized force is exerted on the elastocapillary ridge whenever it is subjected to a deformation field (either its own deformation field or an additional external field, in which case this force is akin to the Peach-Koehler force[82,96]). Equation (3) encompasses both the Young-Dupré relation (for infinitely rigid substrates and no external forces $\vec{f_{ext}} = 0$) as well as the Neumann relation ruling the equilibrium of liquid drops over a liquid bath (in the limit of a substrate with vanishing shear and no external forces $\vec{f_{ext}} = \vec{f}_s = 0$). In the general case however, the equilibrium angle of static droplets on soft substrates does not obey either of these two laws but satisfies Eq. (3).

In this paper, we show that Eq. (3) can also help predicting the out-of-equilibrium value of the contact angle selected during the motion of inviscid drops at constant velocities at the free surface of viscoelastic substrates. In section 2, we provide a derivation of the generalized force balance Eq. (3) using a variational principle. This section draws inspiration from Maugin's pioneering work[97,98] and we hope that it is as self-contained as possible. The reader already familiar with the nonlinear theory of continuum mechanics may skip directly to section 3.

In section 3 we show that both nonlinear localized capillary forces and visco-elastic stresses oppose the motion of the contact line. We give an explicit analytic formula relating the dynamic contact angle of a moving contact line with its velocity for arbitrary rheology. We then specialize this formula to the experimentally relevant case of elastomers with a Chasset-Thirion (power-law) type of rheologies. The resulting theoretical predictions are in excellent agreement with experimental data[59,60]: they capture the saturation of the dynamic contact angle at high velocities, without any adjustable parameters, for example. In section IV, we show that Eq. (3) can also be used to recover the classical de Gennes model[3] of dynamical wetting for a viscous drop moving over a hard substrate by choosing a contour Γ located inside a liquid wedge moving at constant velocity. In section V, we investigate the as-yet largely unexplored case of a viscous fluid spreading over a visco-elastic substrate and we give predictions for the selection of the dynamic contact angle for such systems. Finally, we conclude the paper with a discussion of the nonlinear elastowetting problem in section VI.

2 Formulation of the nonlinear elastowetting problem

The purpose of this section is to provide the reader with the concepts and tools of nonlinear continuum mechanics[99] necessary to the understanding of this paper as well as a derivation of Eq. (3). We start by reminding the reader with the expression of stress balances describing the equilibrium of a body in its initial (reference) configuration and its deformed (current) configuration, and their relationship, and we obtain the appropriate form of the variational principle. As the treatment of the wetting of a soft substrate by a liquid requires to account for a jump in the strain field, we then discuss the form of the variational principle when a discontinuity is present. Finally, we add the contribution of surface energy.

2.1 General stress balance at equilibrium in nonlinear continuum mechanics

We consider an elastic body $B \in \Re^3$ in the reference configuration $\mathscr{B}_0$. Granted coherency (no material interpenetration or cavitation), the deformation is described by an invertible continuous mapping $\chi : \mathscr{B}_0 \mapsto \mathscr{B}$ that transforms the material point $\vec{X} \in \mathscr{B}_0$ to a position $\vec{x} = \chi(\vec{X})$ in the current configuration $\mathscr{B}$ (Fig. 2). A local description of this deformation is provided by the deformation tensor $\mathbf{F} = \partial\vec{x}/\partial\vec{X}$. The body experiences some tractions $\vec{T}^d(\vec{X})$ at the boundary $\partial\mathscr{B}_0$ in the reference configuration.

We wish to find the equilibrium state of the solid in response to these external tractions. The next steps rely on a thermodynamic approach. First, we place ourselves in the context of Green elasticity (or hyperelasticity) and assume the existence of a strain energy density $\mathscr{W}(\mathbf{F})$. Given the presence of tractions at the free surface of B , the energy functional of the system is:

$$\mathscr{E}[\vec{x}] = \int_{\mathscr{B}_0} \mathscr{W}(\mathbf{F})\mathrm{d}V - \int_{\partial\mathscr{B}_0} \vec{T}^d . \vec{x}\,\mathrm{d}A.$$

The principle of stationary potential energy stipulates that the material variation δ_X (where the subscript specifies that the variation must be performed at fixed $\vec{X}$) of the energy functional $\mathscr{E}[\vec{x}]$ is zero at equilibrium, $\delta_X\mathscr{E}[\vec{x}] = 0$. Any deformation field $\vec{x} = \chi(\vec{X})$ that renders the energy functional stationary is known as an extremal. Because the material variation δ_X conserves the material volume and commutes with the material space integration, we have:

$$\begin{aligned}
\delta_X\mathscr{E}[\vec{x}] &= \int_{\mathscr{B}_0} \delta_X\mathscr{W}(\mathbf{F})\mathrm{d}V - \int_{\partial\mathscr{B}_0} \vec{T}^d . \delta_X\vec{x}\,\mathrm{d}A && (5a)\\
&= \int_{\mathscr{B}_0} \frac{\partial\mathscr{W}}{\partial\mathbf{F}}\delta_X\mathbf{F}\mathrm{d}V - \int_{\partial\mathscr{B}_0} \vec{T}^d . \delta_X\vec{x}\,\mathrm{d}A && (5b)\\
&= \int_{\mathscr{B}_0} \nabla_X\left(\frac{\partial\mathscr{W}}{\partial\mathbf{F}}\delta_X\vec{x}\right)\mathrm{d}V - \int_{\mathscr{B}_0} \nabla_X\left(\frac{\partial\mathscr{W}}{\partial\mathbf{F}}\right)\delta_X\vec{x}\mathrm{d}V\\
&\quad - \int_{\partial\mathscr{B}_0} \vec{T}^d . \delta_X\vec{x}\,\mathrm{d}A && (5c)
\end{aligned}$$

where integration by parts has been used between Eqs.(5b) and (5c). Defining the nominal stress tensor $\mathbf{S} \equiv \partial\mathscr{W}/\partial\mathbf{F}$, and under the condition that $\mathbf{S}$ is a continuously differentiable tensor field, transformation of the first volume integral appearing in the r.h.s. of Eq. (5c) into a surface integral using Gauss's theorem leads to:

$$\int_{\mathscr{B}_0} \nabla_X\left(\frac{\partial\mathscr{W}}{\partial\mathbf{F}}\delta_X\vec{x}\right)\mathrm{d}V = \int_{\partial\mathscr{B}_0} \left(\mathbf{S}^T\vec{N}\right).\delta_X\vec{x}\mathrm{d}A. \qquad (6)$$

where $\vec{N}$ is the outward unit vector normal to the reference boundary $\partial\mathscr{B}_0$ of the body and $\mathbf{S}^T$ denotes the transpose of $\mathbf{S}$. The arbitrariness of the $\delta_X\vec{x}$ leads us to the local form of the equilibrium equations in the reference configuration $\mathscr{B}_0$:

$$\nabla_X\mathbf{S} = \vec{0} \text{ in } \mathscr{B}_0 \qquad (7)$$

$$\mathbf{S}^T\vec{N} = \vec{T}^d \text{ on } \partial\mathscr{B}_0 \qquad (8)$$

The equilibrium equation (7) together with the traction boundary condition (8) can also be rewritten in the current configuration $\mathscr{B}$. We first rewrite Eq. (5c) in compact form using

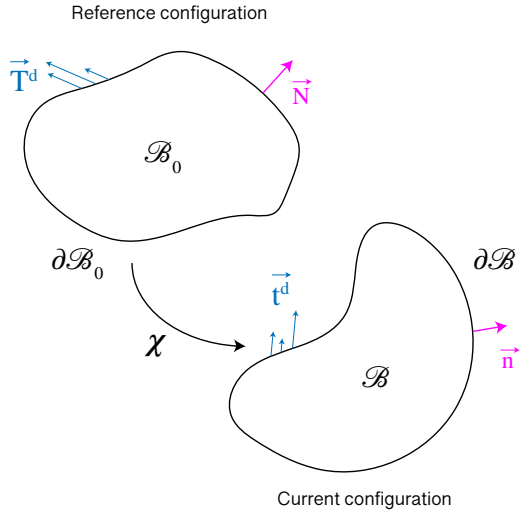

Fig. 2 Schematic of the change from the reference configuration of an elastic body to its current configuration after finite-strain deformation. The elastic body B is subjected to a distribution of surface tractions $\vec{T}^d(\vec{X})$ in the reference configuration $\mathscr{B}_0$ with boundary $\partial\mathscr{B}_0$. The unit vector $\vec{N}$ is normal to the reference boundary $\partial\mathscr{B}_0$ and points toward the exterior of the body B. After the deformation, described by the mapping χ, the body is in the current configuration $\mathscr{B}$ and is bounded by the boundary $\partial\mathscr{B}$. The surface tractions in $\mathscr{B}$ are noted $\vec{t}^d$. The unit vector $\vec{n}$ is normal to the current boundary $\partial\mathscr{B}$ and points toward the exterior of the body B.

Eq. (6):

$$\delta_X\mathscr{E}[\vec{x}] = \int_{\partial\mathscr{B}_0} \left(\mathbf{S}^T\vec{N} - \vec{T}^d\right).\delta_X\vec{x}\mathrm{d}A - \int_{\mathscr{B}_0} (\nabla_X\mathbf{S})\,\delta_X\vec{x}\mathrm{d}V \qquad (9)$$

Let us recall Nanson's formula that connects the surface elements in the reference and deformed configurations:

$$\vec{n}\mathrm{d}a = J\mathbf{F}^{-T}\vec{N}\mathrm{d}A$$

where $\vec{n}$ is the outward unit vector normal to the current boundary $\partial\mathscr{B}$ of the body, $J \equiv \det\mathbf{F}$ is the determinant of the tensor $\mathbf{F}$ and $\mathbf{F}^{-T}$ denotes the inverse of the transpose of $\mathbf{F}$. Defining the Cauchy stress tensor as $\mathbf{T} = J^{-1}\mathbf{F}\mathbf{S}$ and making use of the balance of rotational momentum $\mathbf{T}^T = \mathbf{T}$, the first integral in the r.h.s. of (9) can be rewritten as an integral over the current boundary $\partial\mathscr{B}$ of the body:

$$\int_{\partial\mathscr{B}_0} \left(\mathbf{S}^T\vec{N} - \vec{T}^d\right).\delta_X\vec{x}\mathrm{d}A = \int_{\partial\mathscr{B}} \left(\mathbf{T}\vec{n} - \vec{t}^d\right).\delta_X\vec{x}\mathrm{d}a \qquad (10)$$

where we have defined the traction applied on the current boundary $\partial\mathscr{B}$ as $\vec{t}^d = \vec{T}^d J\vec{N}\mathbf{F}^T\vec{n}$. Now using the formula for volume change $\mathrm{d}v = J\mathrm{d}V$, as well as the identity $\nabla_X.(J\mathbf{F}^{-1}) = \vec{0}$, it follows immediately that:

$$\int_{\mathscr{B}_0} (\nabla_X\mathbf{S})\,\delta_X\vec{x}\mathrm{d}V = \int_{\mathscr{B}} (\nabla_x\mathbf{T})\,\delta_X\vec{x}\mathrm{d}v \qquad (11)$$

Injecting (10) and (11) into equation (9), we thus obtain the local equilibrium equations in the current configuration:

$$\nabla_x\mathbf{T} = \vec{0} \text{ in } \mathscr{B} \qquad (12)$$

$$\mathbf{T}\vec{n} = \vec{t}^d \text{ on } \partial\mathscr{B} \qquad (13)$$

Note that either (7)-(8) or (12)-(13) are valid provided that $\mathbf{S}$, $\mathbf{T}$ and $\mathbf{F}$ are continuously differentiable tensor fields.

2.2 Variational principle for discontinuous fields: stress balance for an elastic body at equilibrium in the presence of a discontinuity.

In many situations however, the boundary value problems (7)-(8) or (12)-(13) do not possess any solution (or extremal), with the required degree of smoothness. In this case, one may try to relax some of the smoothness requirements and look for *broken* extremals instead. A broken extremal is a solution of (7)-(8) or (12)-(13) in which some of the fields of interest ($\vec{x}$, $\mathbf{S}$, $\mathbf{T}$, $\mathbf{F}$, etc) are allowed to have local discontinuities. Of course true discontinuities seldom occur in experiments and these discontinuities must be physically interpreted as abrupt changes across a transition zone whose extent compared to other typical length scales of the problem is small and where additional physics come into play.

However, such broken extremals are typically not uniquely defined and additional constraints must be enforced to find a unique solution to the boundary value problems (7)-(8) or (12)-(13). One possible approach to solve this underdetermination consists in introducing a small inner zone where these additional physical mechanisms are specified. If a solution of the inner problem is found, then one attempt to match it to the outer solution (the broken extremal). In favorable situations, this matching procedure resolves the underdetermination and a unique solution is found. In the elastowetting problem at hand, the width of this inner zone is the width of the contact line. Although this quantity is so far unknown experimentally, X-ray and confocal measurements gives an upper bound of the order of a few tens of nanometer[52,62,63]. Because the continuum mechanics framework will break at such scales, the physics describing the behavior of the inner zone is likely to involve a molecular theory. Of course, because elastic deformations are large, all (material and geometric) nonlinearities should then be taken into account, both in the inner and outer zones. A matching between a nonlinear molecular theory at small scales and a nonlinear continuous theory at large scale is a difficult approach that we shall not attempt in this work. Instead, we will take another route that we now introduce.

Rather than specifying some additional physical mechanisms in the transition zone, we will use the framework of nonlinear elasticity with discontinuous fields[97,98] and look for true broken extremals. In what follows, we thus treat the sharp variation across the transition zone as a true discontinuity, or a *defect*. Said otherwise we will consider that those sharp variations occur over a region of vanishing width. The discontinuity may then be a point, a line or a surface embedded in $\mathfrak{R}^3$. As mentioned above, some additional constraints must be specified across the discontinuity in order to obtain a unique solution. As we shall see below, those constraints are obtained, loosely speaking, by minimizing the energy functional with respect to the position of the discontinuity. Because this minimization can be performed either with respect to the deformed position or to the reference position of the defect, it yields two sets of constraints known as the Weierstrass-Erdmann jump conditions. Of course, in the presence of discontinuities, the derivation presented in the previous paragraph fails from the mathematical standpoint and some modifications must be made in order to expand the class of admissible solutions and derive the associated Weierstrass-Erdmann jump conditions.

Note that besides the elastowetting problem studied here, broken extremals and their associated Weierstrass-Erdmann jump conditions have a very long history in physics, starting with the pioneering work of Poisson in the early nineteenth century[100]. They arise in numerous problems of continuum mechanics such as shock waves[101–103], phase-transformation fronts[104,105], plasticity[106], but also in various extremization problems in physics. The most notable example of a broken extremal is the path of a light ray at an interface between two media with different refractive indices. Remarkably, the Weierstrass-Erdmann condition at the surface of discontinuity turns out to be none other than the celebrated Snell-Descartes law.

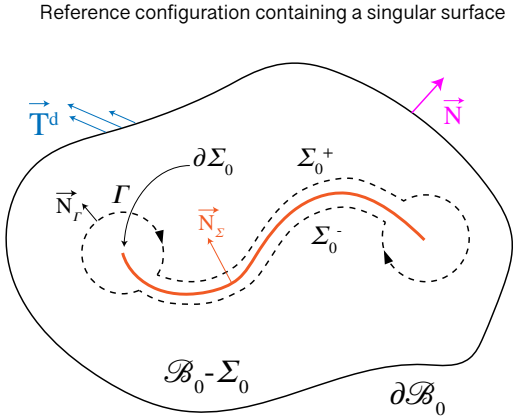

Fig. 3 Reference configuration of an elastic body containing a singular surface. An elastic body B containing a singular surface Σ_0 with boundary $\partial\Sigma_0$ is subjected to a distribution of surface tractions $\vec{T}^d(\vec{X})$ in the reference configuration $\mathcal{B}_0$ with boundary $\partial\mathcal{B}_0$. The unit vector $\vec{N}$ is normal to the reference boundary $\partial\mathcal{B}_0$ and points toward the exterior of the body B. Inspired by[107].

We illustrate the use of broken extremals with the description of the equilibrium of an elastic body containing a surface of discontinuity of finite extent Σ_0 and regular boundary $\partial\Sigma_0$ in the reference configuration (Fig. 3). Following Maugin[97,98,107], we exclude the surface of discontinuity from the domain of interest and define $\mathscr{E}|_{\Sigma_0}$ (respectively $\mathscr{W}|_{\Sigma_0}$) as the restriction of $\mathscr{E}$ (respectively $\mathscr{W}$) to the domain $\mathcal{B}_0 - \Sigma_0$:

$$\mathscr{E}|_{\Sigma_0}[\vec{x}] = \int_{\mathcal{B}_0-\Sigma_0} \mathscr{W}|_{\Sigma_0}(\mathbf{F})\mathrm{d}V - \int_{\partial\mathcal{B}_0} \vec{T}^d.\vec{x}\,\mathrm{d}A \qquad (14)$$

We now apply the principle of stationary potential energy to $\mathscr{E}|_{\Sigma_0}$. Because $\mathscr{W}|_{\Sigma_0}$ does not contain any singularity, we repeat the calculation leading to Eq. (5c) and we obtain:

$$\begin{aligned}\delta\mathscr{E}|_{\Sigma_0}[\vec{x}] \;=\; & \int_{\mathcal{B}_0-\Sigma_0} \nabla_X\left(\frac{\partial\mathscr{W}|_{\Sigma_0}}{\partial\mathbf{F}}\delta_X\vec{x}\right)\mathrm{d}V \\ & - \int_{\mathcal{B}_0-\Sigma_0} \nabla_X\left(\frac{\partial\mathscr{W}|_{\Sigma_0}}{\partial\mathbf{F}}\right)\delta_X\vec{x}\mathrm{d}V \\ & - \int_{\partial\mathcal{B}_0} \vec{T}^d.\delta_X\vec{x}\,\mathrm{d}A \qquad (15)\end{aligned}$$

The transformation of the first volume integral appearing in the r.h.s. of Eq. (15) into a surface integral is difficult. We need a generalization of Gauss's theorem. To do so, we enclose the finite surface Σ with by a closed surface made of a torus-like tube enclosing the boundary $\partial\Sigma_0$ and connected with two surfaces enclosing the singular surface Σ_0[107]. The generalization

reads:

$$\int_{\mathscr{B}_0-\Sigma_0}\nabla_X\left(\frac{\partial\mathscr{W}|_{\Sigma_0}}{\partial\mathbf{F}}\delta_X\vec{x}\right)\mathrm{d}V = \int_{\partial\mathscr{B}_0}\left(\mathbf{S}^T\vec{N}\right)\delta_X\vec{x}\mathrm{d}A + \int_{\partial\Sigma_0}\left(\lim_{\Gamma\to0}\int_\Gamma\mathbf{S}^T\vec{N}_\Gamma\mathrm{d}\Gamma\right)\delta_X\vec{x}\mathrm{d}L - \int_{\Sigma_0}[\mathbf{S}^T]\vec{N}_\Sigma\delta_X\vec{x}\mathrm{d}A \quad (16)$$

where we keep the notation $\mathbf{S}$ for the nominal stress tensor, here defined as $\mathbf{S}\equiv\partial\mathscr{W}|_{\Sigma_0}/\partial\mathbf{F}$, to avoid notation overload. In Eq.(16), the bracket operator $[\mathbf{A}(\vec{X})]$ denotes the finite jump of the field $\mathbf{A}(\vec{X})$ defined as:

$$[\mathbf{A}(\vec{X})]\equiv A^+-A^-$$

where $A^\pm$ is the uniform limit of $\mathbf{A}(\vec{X})$ when approaching Σ_0 from the positive or negative side of Σ_0, along its normal $\vec{N}_\Sigma$ that is oriented from the negative side Σ_0^- to the positive side Σ_0^+ of Σ_0. Γ is the cross-sectional circuit, in the indirect (clockwise) sense, around a section of the torus-like tube enclosing $\partial\Sigma_0$.

We now inject Eq. (16) in Eq. (15) to obtain the local form of the variational principle in the presence of a discontinuity in the reference configuration:

$$\nabla_X\mathbf{S} = \vec{0}\text{ in }\mathscr{B}_0-\Sigma_0 \quad (17)$$

$$\mathbf{S}^T\vec{N} = \vec{T}^d\text{ on }\partial\mathscr{B}_0 \quad (18)$$

$$\left[\mathbf{S}^T\right]\vec{N}_\Sigma = \vec{0}\text{ across }\Sigma_0 \quad (19)$$

$$\lim_{\Gamma\to0}\int_\Gamma\mathbf{S}^T\vec{N}_\Gamma\mathrm{d}\Gamma = \vec{0}\text{ on }\partial\Sigma_0 \quad (20)$$

Equations (17) and (18) are the equilibrium-equation and traction-boundary-condition (*i.e.* equivalents of equations (7)-(8) restricted to the domain $\mathscr{B}_0-\Sigma_0$). Equation (19) imposes the continuity of tractions across the singular surface Σ_0 while Eq. (20) is a condition on the nature of the singularity (if any is present in the body) at the boundary $\partial\Sigma_0$. These two identities form the first Weierstrass-Erdmann condition, here expressed for the case of a 2D discontinuity surface of finite extent embedded in a three-dimensional body. If the discontinuity is a surface of infinite extent, then only Eq. (19) is relevant while for a line discontinuity only Eq. (20) is used. Following the same procedure leading from Eqs.(7)-(8) to Eqs.(12)-(13), Eqs.(17) to (20) can also be rewritten to obtain the local form of the variational principle in the presence of a discontinuity in the current configuration:

$$\nabla_x\mathbf{T} = \vec{0}\text{ in }\mathscr{B}-\Sigma \quad (21)$$

$$\mathbf{T}\vec{n} = \vec{t}^d\text{ on }\partial\mathscr{B} \quad (22)$$

$$[\mathbf{T}]\vec{n}_\Sigma = \vec{0}\text{ across }\Sigma \quad (23)$$

$$\lim_{\Gamma\to0}\int_\Gamma\mathbf{T}\vec{n}_\Gamma\mathrm{d}\Gamma = \vec{0}\text{ on }\partial\Sigma \quad (24)$$

2.3 Variational formulation of the elastowetting problem: accounting for surface energy

So far we have not associated any surface energy with either the boundary $\partial\mathscr{B}_0$ or with the surface of discontinuity Σ_0. However, a surface energy will be associated with $\partial\mathscr{B}_0$ in many instances such as elastowetting. Then, additional surface terms will appear in the energy functional Eq. (14) and in the boundary condition Eq. (18) as well as in the traction continuity conditions Eqs.(19)-(20).

We shall now derive the local form of the variational principle in the presence of a discontinuity for an elastic body that has a surface energy. For the sake of simplicity, we focus on the simple case where the discontinuity is a straight one-dimensional line (such as the triple line), denoted $\mathscr{L}$ (respectively $\mathscr{L}_0$) in the current (respectively reference) configuration, embedded at the free surface of a three-dimensional space. In this framework, the force $\vec{t}^{\,\mathrm{d}}(\vec{x})$ appearing at the r.h.s. of Eq. (22) can be rewritten as a force per unit of length of $\mathscr{L}$ $\vec{\gamma}_{\ell\mathrm{v}}$ applied on the current contact line $\mathscr{L}$. The contact line $\mathscr{L}$ partitions the current boundary $\partial\mathscr{B}$ of the body into two disjoints surfaces $\partial\mathscr{B}^1$ and $\partial\mathscr{B}^2$. These surfaces correspond to the solid-liquid and solid-vapor interfaces, and their surface energies are different in general. We assume that the body is made of a soft material such as an elastomer the surface energy γ_s of which we have argued to be strain-independent and equal to that of the base liquids. If we define $\gamma_{\mathrm{s}1}$ and $\gamma_{\mathrm{s}2}$ the surface energies of the solid-liquid and solid-vapor interfaces, the energy functional $\mathscr{E}_{\mathscr{L}_0}[\vec{x}]$ is:

$$\mathscr{E}_{\mathscr{L}_0}[\vec{x}] = \int_{\mathscr{B}_0-\mathscr{L}_0}\mathscr{W}|_{\mathscr{L}_0}(\mathbf{F})\mathrm{d}V-\int_{\mathscr{L}}\vec{\gamma}_{\ell\mathrm{v}}.\vec{x}\,\mathrm{d}\ell + \int_{\partial\mathscr{B}^1}\gamma_{\mathrm{s}1}\mathrm{d}a+\int_{\partial\mathscr{B}^2}\gamma_{\mathrm{s}2}\mathrm{d}a \quad (25)$$

Now, we evaluate the variational derivative of Eq. (25) to obtain the local form of the variational principle, keeping in mind that the deformed domains $\partial\mathscr{B}^1$, $\partial\mathscr{B}^2$ and $\mathscr{L}$ are of course themselves functions of the displacement field $\vec{x}$. From the properties of the shape derivative[108], we have the following result:

$$\delta_X\int_{\partial\mathscr{B}^\mathrm{i}}\gamma_{\mathrm{si}}\mathrm{d}a=-\int_{\partial\mathscr{B}^\mathrm{i}}\gamma_{\mathrm{si}}\vec{n}\cdot(\nabla_x\vec{n})\delta_X\vec{x}\mathrm{d}a-\int_{\mathscr{L}}\vec{\gamma}_{\mathrm{si}}.\delta_X\vec{x}\,\mathrm{d}\ell$$

where we have defined the vector $\vec{\gamma}_{\mathrm{si}}\equiv\gamma_{\mathrm{si}}\vec{t}_{\mathscr{L}^\mathrm{i}}$ with $\vec{t}_{\mathscr{L}^\mathrm{i}}$ the inward unit vector locally tangent to the boundary $\partial\mathscr{B}^\mathrm{i}$ of the body at the contact line $\mathscr{L}$ and directed from the $\mathscr{L}$ toward the interior of $\partial\mathscr{B}^\mathrm{i}$. The variation of the remaining terms in the r.h.s. of (25) are performed as in (15) and (16) and then converted in integrals over the current domain following the same procedure as in (10) and (11). Written in local form, the equilibrium description of an elastic body in the presence of a single contact line is:

$$\nabla_x\mathbf{T} = \vec{0}\text{ in }\mathscr{B}-\mathscr{L} \quad (26)$$

$$\mathbf{T}\vec{n} = \gamma_{\mathrm{s}1}\vec{n}\cdot(\nabla_x\vec{n})\text{ on }\partial\mathscr{B}^1 \quad (27)$$

$$\mathbf{T}\vec{n} = \gamma_{\mathrm{s}2}\vec{n}\cdot(\nabla_x\vec{n})\text{ on }\partial\mathscr{B}^2 \quad (28)$$

$$\lim_{\Gamma\to0}\int_\Gamma\mathbf{T}\vec{n}_\Gamma\mathrm{d}\Gamma = \vec{\gamma}_{\ell\mathrm{v}}+\vec{\gamma}_{\mathrm{s}1}+\vec{\gamma}_{\mathrm{s}2}\text{ on }\mathscr{L}. \quad (29)$$

Equation (29) is the nonlinear force balance Eq. (3) presented in the introduction. Note that, according to Batra[109], the l.h.s. of (29) can also be rewritten in term of the Eshelby stress tensor ($\mathscr{W}|_{\mathscr{L}_0}\mathbf{I}-\mathbf{SF}$). The results above are independent of a

specific constitutive equation and they are therefore valid for arbitrarily large deformations and arbitrary materials. We have shown in a recent work[82] that solutions to the system (26-29) are able to capture available data on the dependence of the shape of the ridge on strains applied to the elastomer[75]. An interesting outcome of the success of this model is that plasticity seems to be unimportant to describe elastowetting in contrast to early suggestions[61].

The equations that we have derived in Sec. 2.2 and 2.3 describe systems for which the position of the contact line is prescribed, either in the reference or current configuration such as pinned static contact lines and the contact lines moving in a prescribed fashion (for example at constant velocity). In the more general case, the contact line is free to move: its lateral position is not prescribed by the experiments or by the symmetries of the system. Then this position is an additional unknown quantity that must be solved for together with the force balance presented above. An additional scalar equation is needed to close the system. This equation is simply given by the minimization of the energy functional (25) with respect to the lateral position of the contact line (again this minimization can be carried either in the reference or current configuration). This minimization leads to a balance of force known as the configurational force balance at the ridge tip, or the second Weierstrass-Erdmann condition, involving as one may expect the Eshelby stress tensor. While the study of this configurational force balance is outside the scope of this paper we will present shortly thereafter a simple connection between the Eshelby and Cauchy stress tensors valid for disclination-like defects.

3 Spreading of a liquid on a compliant substrate: the nonlinear dynamics of elastowetting.

Now we turn to the dynamics of elastowetting, in which a drop of viscous fluid spreads at the free surface of a viscoelastic material. This work is motivated by available experimental data. We assume that the substrate is a linearly viscoelastic material that again does not experience plasticity. For such a material, all the various stress measures (such as the Cauchy stress tensor $\mathbf{T}$ and the nominal stress tensor $\mathbf{S}$) reduce to the same viscoelastic linear stress measure $\boldsymbol{\sigma}$ that we define below. We investigate the effects of the geometric nonlinearities that arise in the boundary-value-problem defined by Eqs. (26) to (29).

3.1 An inviscid drop moving over a soft visco-elastic substrate

Energy dissipation in the most general case of a droplet spreading on a soft viscoelastic substrate may occur in both the liquid and the solid. However, most experiments look at the spreading of water on an elastomer. Dissipation in the former can then be argued to be much smaller than that in the latter. As a consequence, we restrict our model to the case of an inviscid fluid spreading on a viscoelastic substrate.

We start by considering a single contact line moving with a constant velocity V and a dynamic contact angle $\theta_{\rm dyn}$ at the free surface of an initially flat, incompressible, linearly viscoelastic layer with thickness H (Fig. 4). The reference state of the layer is described in cartesian coordinates by the region $-\infty < x < \infty$ and $-H < y < 0$. The moving contact line deforms the layer and

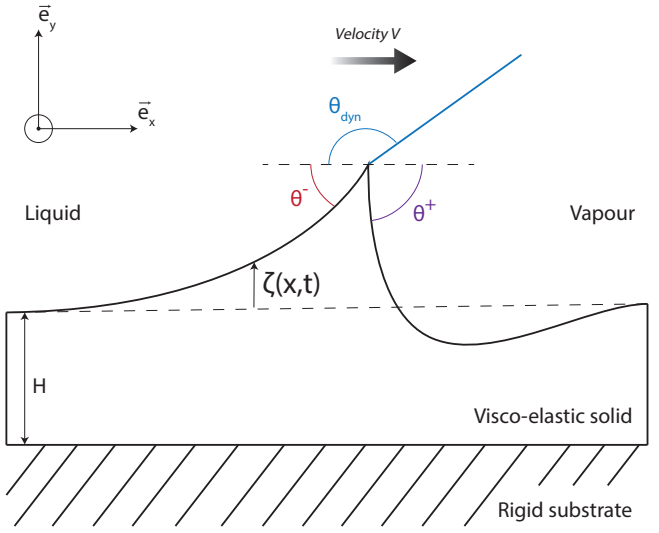

Fig. 4 A liquid drop with surface tension γ_ℓ moves at constant velocity V over a viscoelastic layer with initial thickness H and surface tension γ_s. The drop is located on the left of the contact line and advances with a dynamic contact $\theta_{\rm dyn}$ with the horizontal. The surface deformation of the viscoelastic layer is denoted by the function $\zeta(x,t)$. The slope of the interface has a jump discontinuity at the contact line. The angles $\theta^- = |\partial\zeta/\partial x|_{x=Vt^-}|$ and $\theta^+ = |\partial\zeta/\partial x|_{x=Vt^+}|$ are the positive slopes of the solid surface on each side of the triple line located at $x = Vt$.

maps material points initially located at $\vec{x} = \{x,y\}$ to a new position $\vec{\chi}(\vec{x},t) = \vec{x} + \vec{u}(\vec{x},t)$ where $\vec{u}(\vec{x},t) = \{u_x(\vec{x},t), u_y(\vec{x},t)\}$ is the displacement field. The liquid has a surface tension $\gamma_\ell \equiv |\vec{\gamma}_{\ell v}|$ and we assume for simplicity that the solid has a constant uniform surface tension $\gamma_s \equiv |\vec{\gamma}_{sv}| = |\vec{\gamma}_{s\ell}|$. In other words, the static equilibrium contact angle is $\theta_{\rm eq} = \pi/2$. We further assume that the stress $\boldsymbol{\sigma}(\vec{x},t)$ and strain $\boldsymbol{\varepsilon}(\vec{x},t) = \partial\vec{u}/\partial\vec{x}$ tensors in the soft layer are related by the following general constitutive equation, valid for arbitrary linear viscoelastic materials:

$$\boldsymbol{\sigma}(\vec{x},t) = \int_{-\infty}^{t} \mu(t-t') \frac{\partial \boldsymbol{\varepsilon}}{\partial t'} \mathrm{d}t' - p(\vec{x},t)\boldsymbol{I}, \tag{30}$$

where $\boldsymbol{I}$ is the identity matrix. The pressure $p(\vec{x},t)$ is the Lagrange multiplier associated with the incompressibility constraint. For stationary contact lines, the system is described by the following incompressibility condition and balance of linear momentum:

$$\nabla \cdot \vec{u} = 0 \text{ and } \nabla \cdot \boldsymbol{\sigma} = \vec{0}. \tag{31}$$

We close the system of equations (31) with appropriate boundary conditions. Many experimental setups focus on supported elastomer layers that are bound to a more rigid substrate such as a glass slide. As a consequence, we assume that displacements vanish at the lower face of the viscoelastic layer $y = -H$:

$$u_x(x, y = -H, t) = u_y(x, y = -H, t) = 0. \tag{32}$$

Everywhere at the free surface $y = 0$, except at the contact line located at $x = Vt$, the normal projection of the viscoelastic stresses balances the Laplace pressure induced by the curved interface of the solid interface and we have, keeping in mind that the spreading fluid is inviscid:

$$\boldsymbol{\sigma} \cdot \vec{n} = \gamma_s \vec{n} \cdot (\nabla \vec{n}) \text{ at } y = 0 \text{ and } x \neq Vt. \tag{33}$$

At the contact line $(x = Vt, y = 0)$, we apply the general force

balance (3) with $\gamma_{s\ell} = \gamma_{sv} = \gamma_s$ and no external forces, $\vec{f_{ext}} = \vec{0}$. This condition reads, respectively along $\vec{e}_x$ and $\vec{e}_y$:

$$-\gamma_\ell \cos\theta_{dyn} = \gamma_s \left\{\cos\theta^- - \cos\theta^+\right\} + \vec{e}_x \cdot \vec{f}_s, \quad (34a)$$

$$\gamma_\ell \sin\theta_{dyn} = \gamma_s \left\{\sin\theta^- + \sin\theta^+\right\} + \vec{e}_y \cdot \vec{f}_s, \quad (34b)$$

where $\theta^- = |\partial u_y/\partial x(Vt^-,0)|$ and $\theta^+ = |\partial u_y/\partial x(Vt^+,0)|$ are the positive slopes of the solid surface on each side of the triple line located at $x = Vt$ (Fig.2). The force $\vec{f}_s$ exerted by the solid on the triple line is given by Eq. (4). The reader may notice that the sole force exerted by the fluid onto the viscoelastic substrate is located at the contact line and only has a capillary origin: it is due to the liquid-vapor surface energy. In particular, because the fluid is taken here as inviscid, it does not exert any shear on the solid along the liquid-solid interface. We stress again that our analysis is restricted to the stationary motion of triple lines for which the influence of the initial conditions, and in particular the slow growth of the viscoelastic ridge following the deposition of the drop[63], is negligible. In the case of droplets impacting a soft surface, the pulling forces appearing on the l.h.s. of Eqs. (34a) and (34b) must be multiplied by a time-dependent step function $H(t-t_0)$ where t_0 is the time of droplet deposition. Depending on the substrate rheology, such a modification may significantly alter the selection of the dynamic contact angle.

3.2 The linear solution

The boundary-value problem (30)-(31)-(32)-(33)-(34) is posed and we must solve it. Within the framework of a linear theory, the slopes of the deformed solid surface must be small compared to unity for consistency. This condition will be verified when $\gamma_\ell/2\gamma_s \ll 1$. Taking this quantity as a small parameter, we may seek solutions of the system (30) to (34) of the form:

$$\{\vec{u}, p, \boldsymbol{\sigma}, \boldsymbol{\varepsilon}, \vec{f}_s\} = \sum_{i=1}^{\infty} \{\vec{u}^{(i)}, p^{(i)}, \boldsymbol{\sigma}^{(i)}, \boldsymbol{\varepsilon}^{(i)}, \vec{f}_s^{(i)}\} \left(\frac{\gamma_\ell}{2\gamma_s}\right)^i.$$

Although the convergence of the sum above is not guaranteed *a priori*, we have shown recently[82] that the second order theory indeed provides a nice approximation to the numerical solution of the fully nonlinear equations, by contrast with the linear theory. We will therefore keep the same approach here and see wether a second-order theory provides a good description of the available experimental data. Using the expansion above, a double Fourier transform with respect to both time and space yields the first-order solution of the boundary-value problem (30-34). The full solution, given in Appendix A, is equivalent to that of a wedge disclination close to the tip of the ridge[110]. We only provide here the solution for the surface deflection $\zeta(x,t) \equiv (\gamma_\ell/2\gamma_s)\zeta^{(1)}(x,t) \equiv (\gamma_\ell/2\gamma_s)u_y^{(1)}(x,y=0,t)$:

$$\zeta(x,t) = \frac{1}{2\pi}\int_{-\infty}^{\infty} \mathrm{d}k e^{ik(x-Vt)}\hat{\zeta}(k), \quad (35)$$

with

$$\hat{\zeta}(k) = \frac{\gamma_\ell \sin\theta_{dyn}}{\gamma_s}\left[k^2 + F(k)\right]^{-1},$$

and

$$F(k) = \left[\frac{2H^2k^2 + \cosh(2Hk) + 1}{\sinh(2Hk) - 2Hk}\right]\frac{2k\hat{\mu}(-kV)}{\gamma_s}, \quad (36)$$

where we have used the particular definition of $\hat{\mu}(\omega)$:

$$\hat{\mu}(\omega) = i\omega\int_0^\infty \mu(t)e^{-i\omega t}\mathrm{d}t.$$

The solution (35-36) satisfies the boundary-value problem (30-34) at first order in $\gamma_\ell/2\gamma_s$ provided that $\cos\theta_{dyn} = \mathcal{O}(\gamma_\ell/2\gamma_s)$ or, equivalently, that $\theta_{dyn} = \pi/2 + \mathcal{O}(\gamma_\ell/2\gamma_s)$. In particular, let us underline that both components of the first-order force $\vec{f}_s^{(1)}$ vanish. This is due to the fact that the linear solution has an integrable logarithmic singularity near the ridge tip. However, the linear solution (35-36) does not specify the dynamic contact angle beyond the zeroth-order approximation ($\theta_{dyn} = \pi/2$): it only provides the deformed profile of the interface in response to a vertical localized force of magnitude $\gamma_\ell \sin\theta_{dyn}$. This linear solution can be found in several other studies[48,59,60]. The departure of the dynamic contact angle θ_{dyn} from $\pi/2$ results from the fact that the slope of the deformed interface is finite. Said otherwise, it is selected by contributions of higher order in $\gamma_\ell/2\gamma_s$ that we consider in what follows.

3.3 The nonlinear solution: selection of the dynamic contact angle

Let us now write explicitly the boundary-value problem (30-34) at second order. The second-order constitutive relation reads:

$$\boldsymbol{\sigma}^{(2)}(\vec{x},t) = \int_{-\infty}^{t}\mu(t-t')\frac{\partial \boldsymbol{\varepsilon}^{(2)}}{\partial t'}\mathrm{d}t' - p^{(2)}(\vec{x},t)\boldsymbol{I} \quad (37)$$

while the second-order equilibrium equations read:

$$\nabla\cdot\vec{u}^{(2)} = 0 \text{ and } \nabla\cdot\boldsymbol{\sigma}^{(2)} = \vec{0} \quad (38)$$

supplemented by the following boundary condition at the bottom of the viscoelastic layer, at $y = -H$:

$$u_x^{(2)}(x, y=-H, t) = u_y^{(2)}(x, y=-H, t) = 0 \quad (39)$$

while at $y = 0$ and $x \neq Vt$, we have:

$$\sigma_{xy}^{(2)} = -\gamma_s\frac{\partial\zeta^{(1)}}{\partial x}\frac{\partial^2\zeta^{(1)}}{\partial x^2} + \sigma_{xx}^{(1)}\frac{\partial\zeta^{(1)}}{\partial x} \quad (40a)$$

$$\sigma_{yy}^{(2)} = \gamma_s\frac{\partial^2\zeta^{(2)}}{\partial x^2} \quad (40b)$$

where $\sigma_{xx}^{(1)}$ is the first-order stress field associated with the first-order solution $\{\vec{u}^1, p^1\}$. Because the force at the ridge tip involves the stress tensor expressed in the deformed configuration, it is instructive to rewrite the boundary condition at the free surface (40) in the deformed configuration ($x' = x + u_x(x,y), y' = y + u_y(x,y)$):

$$\sigma_{xy}^{(2)} + \frac{\partial\sigma_{xy}^{(1)}}{\partial x'}u^{(1)} + \frac{\partial\sigma_{xy}^{(1)}}{\partial y'}\zeta^{(1)} - \sigma_{xx}^{(1)}\frac{\partial\zeta^{(1)}}{\partial x'} = -\gamma_s\frac{\partial\zeta^{(1)}}{\partial x'}\frac{\partial^2\zeta^{(1)}}{\partial x'^2} \quad (41)$$

$$\sigma_{yy}^{(2)} + \frac{\partial\sigma_{yy}^{(1)}}{\partial x'}u^{(1)} + \frac{\partial\sigma_{yy}^{(1)}}{\partial y'}\zeta^{(1)} = \gamma_s\frac{\partial^2}{\partial x'^2}\left\{\zeta^{(2)} + \frac{\partial\zeta^{(1)}}{\partial x'}u^{(1)}\right\} \quad (42)$$

It can be seen directly from this formulation that the second-order stress tensor will exhibit a singularity stronger than $\sim \log(x)$ in the deformed configuration. Indeed the third term in the l.h.s. of (41) acts as a source of surface shear with a $\sim 1/x'$ singularity. Note that a shift from a logarithmic singularity in

the linear theory to a stronger singularity in a nonlinear framework is expected both from the numerics[82,89,90] and from the analytic solution of the nonlinear Flamant problem[111,112]. At the contact line, $(x = Vt, y = 0)$, we have at second order:

$$-\gamma_\ell \cos\theta_{dyn} = \frac{\gamma_s}{2}\{(\theta^+)^2 - (\theta^-)^2\} + \vec{e}_x \cdot \vec{f_s^{(2)}} \quad (43a)$$

$$0 = \vec{e}_y \cdot \vec{f_s^{(2)}} \quad (43b)$$

Although an analytical solution of the boundary-value-problem (37)-(38)-(39)-(40)-(43) can be obtained, its lengthy expression needs not be recorded here as we are interested only in the second-order restoring viscoelastic force $\vec{f_s^{(2)}}$ acting at the tip of the ridge. In Appendix B, we show that $\vec{f_s^{(2)}}$ is horizontal, *i.e.* $\vec{e}_y \cdot \vec{f_s^{(2)}} = 0$, and given by the following integral:

$$\vec{e}_x \cdot \vec{f_s^{(2)}} = \int_{-\infty}^{\infty} \sigma_{xx}^{(1)} \frac{\partial \zeta}{\partial x} \mathrm{d}x \quad (44)$$

Using Parseval's theorem, we can rewrite Eq. (44) in the frame of the moving ridge as:

$$\vec{e}_x \cdot \vec{f_s^{(2)}} = \frac{\gamma_\ell^2 \sin^2(\theta_{dyn})}{\gamma_s} \Re\left[\int_{-\infty}^{\infty} \frac{ikF_2(k)}{2\pi\gamma_s(k^2+F(k))(k^2+F(-k))})\mathrm{d}k\right]$$

$$\equiv \frac{\gamma_\ell^2 \sin^2(\theta_{dyn})}{\gamma_s} \mathscr{F}_{ve}(H,V,\mu,\gamma_s) \quad (45)$$

where the symbol $\Re$ stands for the real part and $F_2(k)$ is given by:

$$F_2(k) = \left[\frac{-2H^2k^2 + \cosh(2Hk) + 1}{\sinh(2Hk) - 2Hk}\right] \frac{2k\hat{\mu}(-kV)}{\gamma_s},$$

Using the solution (35-36), the restoring capillary force, *i.e.* the first term in the r.h.s. of (43a), can be rewritten as:

$$\frac{\gamma_s}{2}\{(\theta^+)^2 - (\theta^-)^2\} = \frac{\gamma_\ell \sin(\theta_{dyn})}{2}\left(\theta^+ - \theta^-\right)$$

$$= \frac{\gamma_\ell \sin(\theta_{dyn})}{2\pi} \Re\left[\int_{-\infty}^{\infty} -ik\hat{\zeta}(k)\mathrm{d}k\right]$$

$$= \frac{\gamma_\ell^2 \sin^2(\theta_{dyn})}{\gamma_s} \Re\left[\int_{-\infty}^{\infty} \frac{-ik}{2\pi(k^2+F(k))}\mathrm{d}k\right]$$

$$\equiv \frac{\gamma_\ell^2 \sin^2(\theta_{dyn})}{\gamma_s} \mathscr{F}_{cap}(H,V,\mu,\gamma_s) \quad (46)$$

The term $\left(\theta^+ - \theta^-\right)/2$ represents the rotation of the elastocapillary ridge during the motion of the contact line. Also, the reader can notice that expressions (45) and (46) are of the same order $\mathscr{O}(\gamma_\ell/2\gamma_s)^2$, after a division by γ_s. Injecting results (45) and (46) into equation (43a) we obtain:

$$-\gamma_\ell \cos(\theta_{dyn}) = \frac{\gamma_\ell^2 \sin^2(\theta_{dyn})}{\gamma_s} \mathscr{F}_{cap}(H,V,\mu,\gamma_s)$$

$$+ \frac{\gamma_\ell^2 \sin^2(\theta_{dyn})}{\gamma_s} \mathscr{F}_{ve}(H,V,\mu,\gamma_s), \quad (47)$$

that we can rewrite:

$$-\frac{\cos(\theta_{dyn})}{\sin^2(\theta_{dyn})} = \frac{\gamma_\ell}{\gamma_s}\left(\mathscr{F}_{cap}(H,V,\mu,\gamma_s) + \mathscr{F}_{ve}(H,V,\mu,\gamma_s)\right) \quad (48)$$

We deduce from Eq. (48) that the capillary driving force, *i.e.* the l.h.s. of (43a), is resisted not only by the restoring capillary force (46) but also by the viscoelastic force (45). As a consequence, the Neumann construction,*i.e.* Eq. (48) without $\mathscr{F}_{ve}$, does not hold in general during spreading of a liquid on a viscoelastic material.

Relation (48) can be deduced from a global balance of force as well. The total second-order force per unit of length that drives the motion of the contact line and that is applied to the system is $-\gamma_\ell \cos(\theta_{dyn})$. Under the assumption of constant velocity, this tangential force must be balanced by the total resisting shear force, also a second-order quantity since the first-order shear force vanishes, developed by the viscoelastic layer at the free boundary:

$$-\gamma_\ell \cos(\theta_{dyn}) + \int_{-\infty}^{\infty} \sigma_{xy}^{(2)} \mathrm{d}x = 0 \quad (49)$$

which, in view of the boundary condition (40a), is strictly equivalent to (48). Rearranging the terms in (49), we obtain a nonlinear force balance at the contact line in dimensionless form that is identical to Eq. (48):

$$-\frac{\cos(\theta_{dyn})}{\sin^2(\theta_{dyn})} = \frac{\gamma_\ell}{\gamma_s}\left(\mathscr{F}_{cap}(H,V,\mu,\gamma_s) + \mathscr{F}_{ve}(H,V,\mu,\gamma_s)\right) \quad (50)$$

Equation (50) gives the relation between the dynamic contact angle and the velocity of a contact line moving on a substrate of arbitrary rheology and thickness.

We now proceed with the first steps towards a comparison of Eq. (50) with experimental data. We have to choose a constitutive equation for the substrate. A common choice to describe the rheology of the soft layers used in these experiments is the Chasset-Thirion model[113] for which the complex frequency-dependent viscoelastic modulus $\hat{\mu}(\omega)$ is:

$$\hat{\mu}(\omega) = \mu_0(1 + (i\omega\tau)^m)$$

Once this constitutive equation has been specified, it is easily shown that the dimensionless functions $\mathscr{F}_{cap}$ and $\mathscr{F}_{ve}$, which represent respectively the dimensionless capillary and viscoelastic restoring forces, can be written in terms of the dimensionless velocity $\Xi = V\tau/\ell_s$ and dimensionless thickness $\Lambda = H/\ell_s$ where $\ell_s = \gamma_s/(2\mu_0)$ is the elastocapillary length:

$$\mathscr{F}_{cap}(H,V,\mu,\gamma_s) = \mathscr{F}_{cap}\left(\frac{V\tau}{\ell_s}, \frac{H}{\ell_s}\right) \equiv \mathscr{F}_{cap}(\Xi,\Lambda) \quad (51)$$

$$\mathscr{F}_{ve}(H,V,\mu,\gamma_s) = \mathscr{F}_{ve}\left(\frac{V\tau}{\ell_s}, \frac{H}{\ell_s}\right) \equiv \mathscr{F}_{ve}(\Xi,\Lambda) \quad (52)$$

Equation (50) is plotted in Fig. 5A for various values of the dimensionless thickness Λ. For all thicknesses, we observe that the ratio $\cos\theta_{dyn}/\sin\theta_{dyn}{}^2$ increases with Ξ following a power-law behavior. Also, we see that the dynamic contact angle seems to saturate at high velocity. The individual contributions of the capillary $\mathscr{F}_{cap}(\Xi,\Lambda)$ and viscoelastic $\mathscr{F}_{ve}(\Xi,\Lambda)$ restoring forces are plotted in Figure 5-B and are of similar magnitude. In order to better understand the selection of the dynamic contact angle, we investigate analytically the asymptotic behavior of relation (50) in the limit of small ($\Xi = V\tau/\ell_s \ll 1$) and large ($\Xi = V\tau/\ell_s \gg 1$) velocities.

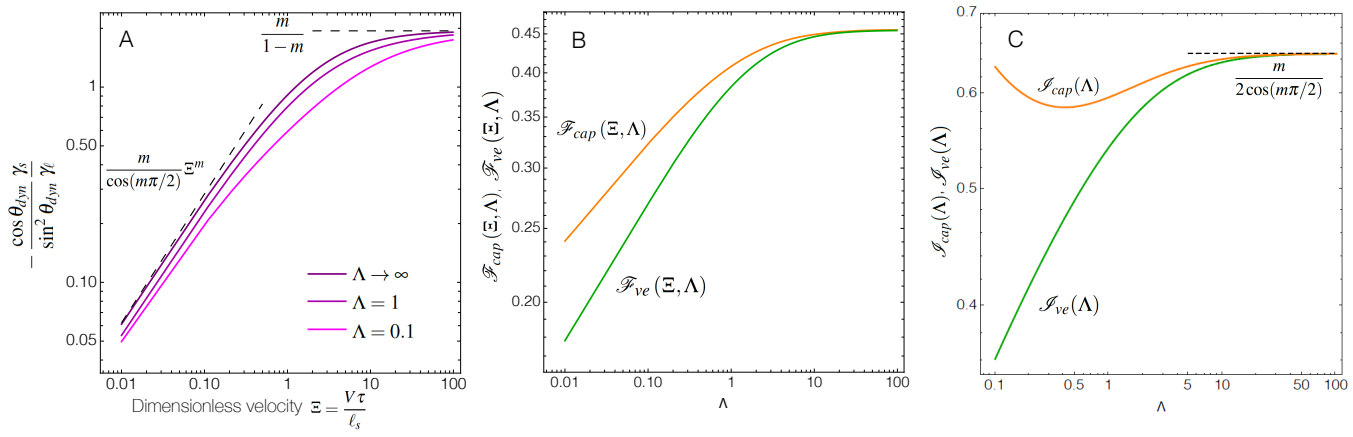

Fig. 5 Results of the nonlinear model of elastowetting. A: Plot in log-log scale of relation (50) between the dynamic contact angle $\theta_{\rm dyn}$ and the dimensionless velocity Ξ for different values of the dimensionless thickness $\Lambda = H/\ell_{\rm s}$ showing the power-law behavior with exponent m at low velocities and saturation of the contact angle at large velocities. B: Plot in log-log scale of the dimensionless functions $\mathscr{F}_{cap}(\Lambda,\Xi)$ and $\mathscr{F}_{ve}(\Lambda,\Xi)$, defined respectively by Eq. (51) and Eq. (52), as functions of the parameter Λ for a fixed value of the dimensionless velocity $\Xi = 1$. $\mathscr{F}_{cap}(\Lambda,\Xi)$ and $\mathscr{F}_{ve}(\Lambda,\Xi)$ capture the dependence of the dynamic contact angle on the aspect ratio Λ of the problem. C: Plot in log-log scale of the dimensionless functions $\mathscr{I}_{cap}(\Lambda)$ and $\mathscr{I}_{ve}(\Lambda)$, defined respectively by Eq. (53) and Eq. (54), that capture the dependance of the dynamic contact angle on the aspect ratio Λ of the problem at low velocities. Both functions converge to $m/(2\cos(m\pi/2))$ in the limit $\Lambda \to \infty$.

3.4 Asymptotic behavior at small velocities Ξ

In this part, we focus on the case $\Xi = V\tau/\ell_s \ll 1$. In this limit, the dimensionless forces $\mathscr{F}_{cap}$ and $\mathscr{F}_{ve}$ admit the following multiplicative decompositions with a power-law dependence on the dimensionless velocity Ξ:

$$\mathscr{F}_{cap}(\Xi,\Lambda) = \mathscr{I}_{cap}(\Lambda)\Xi^m$$

$$\mathscr{F}_{ve}(\Xi,\Lambda) = \mathscr{I}_{ve}(\Lambda)\Xi^m$$

while the influence of the dimensionless thickness $\Lambda = H/\ell_{\rm s}$ on the selection of the dynamic contact angle is captured by the dimensionless functions $\mathscr{I}_{cap}(\Lambda)$ and $\mathscr{I}_{ve}(\Lambda)$ (Fig. 5C):

$$\mathscr{I}_{cap}(\Lambda) = \int_0^\infty \frac{k^m G(k\Lambda)\sin(m\pi/2)}{\pi(k+G(k\Lambda))^2}\mathrm{d}k \tag{53}$$

and

$$\mathscr{I}_{ve}(\Lambda) = \int_0^\infty \frac{k^m \sin(m\pi/2)}{\pi(k+G(k\Lambda))^2}\mathrm{d}k \tag{54}$$

with

$$G(z) = \left[\frac{2z^2+\cosh(2z)+1}{\sinh(2z)-2z}\right]$$

Writing $\mathscr{I}(\Lambda) = \mathscr{I}_{cap}(\Lambda)+\mathscr{I}_{ve}(\Lambda)$, the dynamic force balance may be expressed in the following compact form:

$$-\frac{\cos(\theta_{\rm dyn})}{\sin^2(\theta_{\rm dyn})} = \frac{\gamma_\ell}{\gamma_{\rm s}}\mathscr{I}(\Lambda)\Xi^m \tag{55}$$

In the limit of an infinitely thick substrate ($\Lambda \to \infty$), integrals $\mathscr{I}_{cap}(\Lambda)$ and $\mathscr{I}_{ve}(\Lambda)$ converge to the same limit $m/(2\cos(m\pi/2))$, yielding:

$$\mathscr{I}_\infty \equiv \lim_{\Lambda\to\infty}\mathscr{I}(\Lambda) = 2\lim_{\Lambda\to\infty}\mathscr{I}_{cap}(\Lambda) = \frac{m}{\cos(m\pi/2)}$$

On an infinitely thick substrate, the restoring capillary force and the viscoelastic force thus contribute equally to the horizontal force balance at the moving ridge. In this limit the $\theta_{\rm dyn} - \Xi$ relationship obeys the following equation:

$$-\frac{\cos(\theta_{\rm dyn})}{\sin^2(\theta_{\rm dyn})} = \frac{\gamma_\ell}{\gamma_{\rm s}}\frac{m}{\cos(m\pi/2)}\Xi^m \text{ when } \Lambda\to\infty \tag{56}$$

Figure 5-A shows that relation (56) is in excellent agreement with the general force balance (50) in the limit of small velocities and infinite thickness. The individual contributions of the restoring capillary and viscoelastic forces differ on the other hand for finite values of the aspect ratio Λ (Fig.5C). In particular, the restoring viscoelastic force $\mathscr{I}_{ve}(\Lambda)$ follows the scaling $\sim \Lambda^{3(1-m)/4}$ at small thickness, in agreement with a previous analysis[60].

3.5 Asymptotic behavior at large velocities $\Xi \gg 1$

In the case of large velocities $\Xi \gg 1$, we observe that the contributions to motion resistance of the viscoelastic braking force $\mathscr{F}_{ve}$ and the capillary restoring force $\mathscr{F}_{cap}$ are equal (Fig. 5B) with a magnitude that is independent of the substrate thickness Λ. These contributions read:

$$\lim_{\Xi\to\infty}\mathscr{F}_{cap}(\Xi,\Lambda) = \lim_{\Xi\to\infty}\mathscr{F}_{ve}(\Xi,\Lambda) = \frac{m}{2(1-m)},$$

We therefore obtain the following simple prediction for the maximum achievable dynamic contact angle $\theta_{\rm dyn}^{\max}$:

$$\frac{-\cos(\theta_{\rm dyn}^{\max})}{\sin^2(\theta_{\rm dyn}^{\max})} = \frac{\gamma_\ell}{\gamma_{\rm s}}\frac{m}{1-m} \tag{57}$$

While it is natural to expect the (dimensionless) restoring viscoelastic force $\mathscr{F}_{ve}$ to depend only on the rheology of the material at large enough thickness, it may be surprising that the same result also holds for the (dimensionless) restoring capillary force $\mathscr{F}_{cap}$. This result can be understood by noting that the restoring capillary force is related to the rotation of the elastocapillary ridge as previously noted[59] and shown above. For a purely elastic material the deformation of the ridge is symmetric and no rotation occurs (under the assumptions of neg-

ligible inertia and equal surface energies for the solid-vapour and solid-liquid interfaces). Because of the viscoleasticity of the substrate, the part of the material that has been pulled upward by the contact line takes some time to relax behind the contact line and this delay induces a rotation of the ridge. For a thick enough substrate, this rotation thus only depends on the rheology of the substrate.

3.6 Comparison with experiments

Many of the predictions that we have described in the previous section are reminiscent of experimental observations. For example, saturation of the dynamic contact angle at high velocity has been observed[59]. The prediction that both the restoring capillary force and the resisting viscoelastic force are of comparable order of magnitude may help solving this issue.

Before proceeding with a comparison of the model with experiments, we note that available experimental data on the dynamics of contact lines on soft solids are not obtained with liquids in neutral wetting situation, *i.e.* with $\theta_{eq} = \pi/2$. The equilibrium values are closer to 105°. However Eq. (55) was derived under the hypothesis that the surface energies of the solid-vapour and solid-liquid interfaces are equal. In the general case of broad interest where these quantities are different, the linear problem becomes much more difficult to solve. Although a solution of the linear problem can be found under the form of an infinite series using Sneddon's theory of dual integrals, it is of limited use for the development of an analytical nonlinear theory, as performed in this work.. Thus, we make the assumption that Eq. (55) still holds in the vicinity of an arbitrary equilibrium contact angle. Then we have:

$$\frac{\cos(\theta_{\rm eq}) - \cos(\theta_{\rm dyn})}{\sin^2(\theta_{\rm dyn})} = \frac{\gamma_\ell}{\overline{\gamma_{\rm s}}}\left(\mathscr{F}_{cap}(\Xi,\Lambda) + \mathscr{F}_{ve}(\Xi,\Lambda)\right) \qquad (58)$$

where the reduced thickness $\Lambda = H/\overline{\ell_{\rm s}}$ and velocity $\Xi = V\tau/\overline{\ell_{\rm s}}$ are now defined for consistency based on the effective elasto-capillary length $\overline{\ell_{\rm s}} = \overline{\gamma_{\rm s}}/(2\mu_0)$ where $\overline{\gamma_{\rm s}}$ is an effective value that can be extracted from static experiments[60]. Finally, while the present analysis has been performed for an advancing contact line, it also holds for a receding contact line, simply by changing the sign of the left hand side in Eq. (58).

We compare Eq. (58) to experimental data taken from ref. [60] in Fig. 6-A and B, using the values of the physical parameters given in this reference. Despite the many approximations of our model, and in particular the fact that the static equilibrium contact angle is not $\pi/2$ and that the parameter $\gamma_\ell/(2\overline{\gamma_s}) \sim 0.9$ is not much smaller than unity (and hence terms of order higher than $(\gamma_\ell/2\gamma_s)^2$ might have had a significant contribution), the agreement between theory and experiments is excellent, without any adjustable parameter. In particular, the Ξ^m power law predicted by equation (56) is observed. In Fig. 6-C we also compare the solid opening angle measured in[91] to both our theoretical prediction as well the Neumann triangle construction using the values of the physical parameters they provide, except for the value of the solid surface tension which was not measured independently. Its value was thus fixed at $43\,\mathrm{mN\,m^{-1}}$ in order to fit the value of the opening angle at vanishing velocity. This value is within the error bar of the measurement performed in[60] ($\gamma_s = 42 \pm 2\ \mathrm{mN\,m^{-1}}$) for a similar system. In both cases, the experimental data are very well described by our nonlinear theory while the Neumann construction, *i.e.* Eq. (58) with $\mathscr{F}_{ve} = 0$, fails. Finally, figure 6D shows the relation between $\theta_{\rm dyn} - \theta_{\rm eq}$ and the ridge rotation. Although the agreement between experimental data and either the nonlinear theory (58) or the Neumann construction is poor, the nonlinear theory provides a better description of the experimental data (regression coefficient $R^2 = 0.93$) than the Neumann construction (regression coefficient $R^2 = 0.66$), independently of the value of the solid surface tension $\gamma_{\rm s}$.

We can also compare Eq. (57) with available data for the maximum dynamic contact angle $\theta_{\rm dyn}^{\rm max}$ [59]. Our model predicts $148 \pm 2\ ^\circ$ for $\gamma_{\rm s} = 42 \pm 2\ \mathrm{mN\,m^{-1}}$, a value close to the experimental measurement of $145 \pm 4\ ^\circ$ without any adjustable parameter. By contrast, a model based solely on the balance of surface tensions, *i.e.* the Neuman triangle corresponding to the case $\mathscr{F}_{ve} = 0$, predicts $\theta_{\rm dyn}^{\rm max} = 155 \pm 4\ ^\circ$, overestimating the observed value by 10°, even when taking the surface tension of the solid as a fitting parameter. We therefore conclude from this comparison that it is necessary to take into account the nonlinearities arising from both the capillarity and the viscoelasticity in order to accurately describe the experimental data. We also note that the very good agreement between the theory and the experimental data suggests that the present theory indeed holds for equilibrium contact angles that are not exactly equal to $\pi/2$.

3.7 The global dissipation approach

We provide here for completeness a derivation of the force balance (48) based on a global dissipation approach. Starting from the energy balance equation, and taking into account the fact that the surface energy terms appearing in the energy functional (14) are constant throughout the motion under consideration, global dissipation $\mathscr{D}$ is given by:

$$\mathscr{D} = \frac{\mathrm{d}}{\mathrm{d}t}\int_{\mathscr{B}_0-\mathscr{L}_0} \mathscr{W}|_{\mathscr{L}_0}(\mathbf{F})\mathrm{d}V - \int_{\partial\mathscr{B}_0} \vec{N}\mathbf{S}\frac{\partial\vec{\chi}}{\partial t}\mathrm{d}A - \lim_{\Gamma\to 0}\int_\Gamma \vec{N}_\Gamma\mathbf{S}\frac{\partial\vec{\chi}}{\partial t}\mathrm{d}\Gamma \qquad (59)$$

For a contact line in uniform translation, we have in the steady state regime the following connection:

$$\frac{\partial\vec{\chi}}{\partial t} = -\mathbf{F}\cdot\vec{V}$$

where $\vec{V} = V\vec{e}_x$ is the velocity of the contact line. In order to estimate the first term appearing in the r.h.s. of (59) we make use of the generalized Reynolds theorem to obtain:

$$\begin{aligned}\frac{\mathrm{d}}{\mathrm{d}t}\int_{\mathscr{B}_0-\mathscr{L}_0} \mathscr{W}|_{\mathscr{L}_0}(\mathbf{F})\mathrm{d}V &= \int_{\mathscr{B}_0-\mathscr{L}_0}\frac{\partial\mathscr{W}|_{\mathscr{L}_0}}{\partial t}\mathrm{d}V \\ &\quad - \lim_{\Gamma\to 0}\int_\Gamma \vec{N}_\Gamma\mathscr{W}|_{\mathscr{L}_0}\mathbf{I}\vec{V}\mathrm{d}\Gamma \qquad (60)\end{aligned}$$

Collecting the terms in the expressions above, we obtain the following expression for $\mathscr{D}$:

$$\mathscr{D} = \int_{\mathscr{B}_0-\mathscr{L}_0}\frac{\partial\mathscr{W}|_{\mathscr{L}_0}}{\partial t}\mathrm{d}V + \vec{V}\cdot\left\{-\lim_{\Gamma\to 0}\int_\Gamma \vec{N}_\Gamma\left(\mathscr{W}|_{\mathscr{L}_0}\mathbf{I} - \mathbf{SF}\right)\mathrm{d}\Gamma\right\}$$

in which we recognize the expression for the configurational force $\vec{f}_\Gamma$ acting on a moving singularity:

$$\vec{f}_\Gamma = -\lim_{\Gamma\to 0}\int_\Gamma \vec{N}_\Gamma\left(\mathscr{W}|_{\mathscr{L}_0}\mathbf{I} - \mathbf{SF}\right)\mathrm{d}\Gamma$$

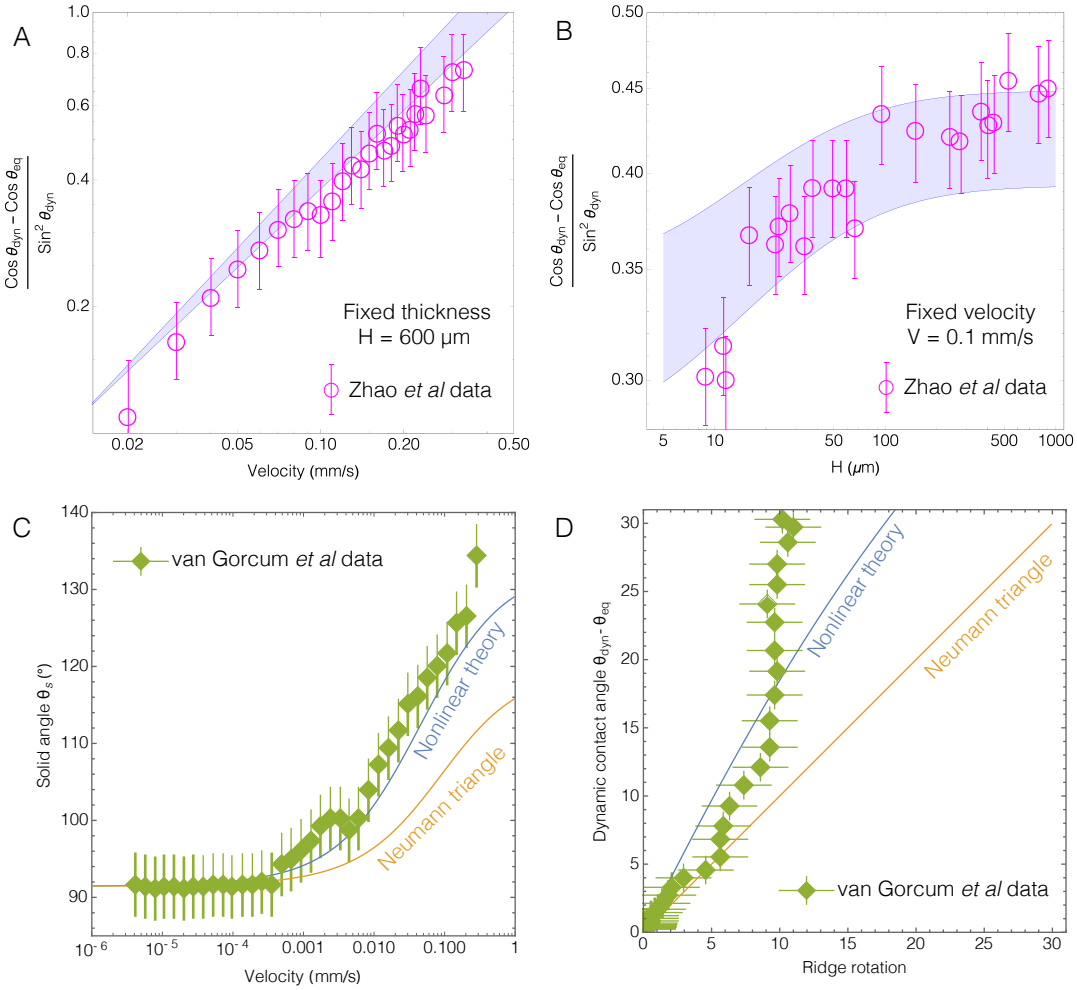

Fig. 6 Comparison of predictions from the nonlinear model of elastowetting with experimental data. A and B: Comparison of experimental data from Zhao *et al.* [60] (magenta circles) with Eq. (50) (blue shaded area) at a fixed thickness of $600\,\mu$m (A) and fixed velocity $0.1\,\mathrm{mm\,s^{-1}}$ (B). Panels A and B are in log-log scale. The values of the physical parameters are taken from ref. [60] and read $\gamma_\ell = 72 \pm 2\,\mathrm{mN\,m^{-1}}$, $\gamma_s = 42 \pm 2\,\mathrm{mN\,m^{-1}}$, $\mu_0 = 1085 \pm 124$ Pa, $\tau = 15.4 \pm 0.4$ ms, m$= 0.66 \pm 0.04$ and $\theta_{eq} = 106 \pm 3°$. The width of the theoretical predictions in B and C reflects the uncertainties in the values of the physical parameters. C and D: Comparison of experimental data from van Gorcum *et al.* [91] (green diamonds) with our nonlinear theory (Eq. (50), blue line) and with the Neumann construction (Eq. (50) with $\mathscr{F}_{ve} = 0$, yellow line) at large thickness $\Lambda \to \infty$. In (C) the solid angle is plotted as a function of the velocity while in (D) the departure of the dynamic contact angle from the static contact angle is plotted as a function of the ridge rotation. The values of the physical parameters (no uncertainties reported) are taken from [91] and read $\gamma_\ell = 72\,\mathrm{mN\,m^{-1}}$, $\mu_0 = 390$ Pa, $\tau = 0.54$ s, m$= 0.58$ and $\theta_{eq} = 105 \pm 2°$. The value of the solid surface tension, not measured independently, was fixed at $\gamma_s = 43\,\mathrm{mN\,m^{-1}}$.

With this notation, the global dissipation can be re-expressed in the classical form:

$$\mathscr{D} = \int_{\mathscr{B}_0 - \mathscr{L}_0} \frac{\partial \mathscr{W}|_{\mathscr{L}_0}}{\partial t} \mathrm{d}V + \vec{V} \cdot \vec{f}_\Gamma$$

The equation above states that the energy is dissipated by viscoelastic stresses within the bulk of the half-space as well as by the configurational force acting on the moving discontinuity. Since energy is injected inside the system by the capillary force at the moving contact line, we obtain the following force balance:

$$(\cos(\theta_{eq}) - \cos(\theta_{dyn}))V = \int_{\mathscr{B}_0 - \mathscr{L}_0} \frac{\partial \mathscr{W}|_{\mathscr{L}_0}}{\partial t} \mathrm{d}V + \vec{V} \cdot \vec{f}_\Gamma \qquad (61)$$

Now, let us note that, on account of the logarithmic singularity of the first-order stress field at the contact line, we have up to second order:

$$\begin{aligned} \vec{f}_\Gamma &= -\lim_{\Gamma \to 0} \int_\Gamma \vec{N}_\Gamma \left(\mathscr{W}|_{\mathscr{L}_0} \mathbf{I} - \mathbf{SF} \right) \mathrm{d}\Gamma \\ &\approx \lim_{\Gamma \to 0} \int_\Gamma \vec{N}_\Gamma \mathbf{S}^{(2)} \mathrm{d}\Gamma \approx \lim_{\Gamma \to 0} \int_\Gamma \vec{N}_\Gamma \mathbf{S} \mathrm{d}\Gamma = \lim_{\Gamma \to 0} \int_\Gamma \vec{n}_\Gamma \mathbf{T} \mathrm{d}\Gamma \end{aligned}$$

The previous relationship implies that, at leading order, the force at the tip of the ridge is given by the integral of either the Cauchy or the Eshelby stress tensor around a contour enclosing the ridge tip. Finally, we may inject the first and second-order solutions derived previously into equation (61) to recover exactly the nonlinear force balance (48).

4 A viscous drop moving over a soft visco-elastic substrate

In this part, we show how our rationale can be extended to the more general case of a viscous droplet moving on a viscoelastic substrate. We first deal with the spreading of a viscous droplet on a rigid elastic substrate. We derive both the De Gennes and

the Cox-Voinov models that describe the shape of the droplet in the vicinity of the moving contact line. We then deal with a viscoelastic substrate, and we identify the existence of an apparent or soft hysteresis in the relation between the contact angle and the capillary number of the experiment. The magnitude of this soft hysteresis depends on the viscoelasticity of the solid.

4.1 De Gennes and Cox-Voinov models of wetting on rigid substrate

We now consider the case of a viscous drop moving on a rigid elastic substrate. Equation (34) can again be used to find the force balance at the contact line. In the limit of an infinitely rigid substrate, the angles θ^- and θ^+ vanish and the vertical capillary traction is balanced solely by the elastic stresses[69]. In the horizontal direction we are thus left with the relation (34a):

$$-\gamma_{\ell \mathrm{v}} \cos(\theta_{\mathrm{dyn}}) + \vec{e}_x \cdot \vec{f_{\mathrm{ext}}} = \gamma_{\mathrm{sv}} - \gamma_{\mathrm{s}\ell} + \vec{e}_x \cdot \vec{f}_{\mathrm{s}}$$

but now the localized force $\vec{f}_{\mathrm{s}}$ must be evaluated by using a contour inside the viscous fluid. As shown by Moffatt[114], in the vicinity of a liquid wedge defined by a free surface moving at velocity V with respect to a solid surface, the fluid flow is self-similar in polar coordinates (r,θ) and can be derived from the stream function $\psi = Vrf(\theta)$. The velocity components (v_r, v_θ) of the fluid flow are:

$$v_r = \frac{1}{r}\frac{\partial \psi}{\partial \theta} = Vf'(\theta), \;\; v_\theta = -\frac{\partial \psi}{\partial r} = -Vf(\theta)$$

where $f(\theta)$ is:

$$f(\theta) = \frac{\theta\cos(\theta)\sin(\theta_{\mathrm{dyn}}) - \theta_{\mathrm{dyn}}\cos(\theta_{\mathrm{dyn}})\sin(\theta)}{\sin(\theta_{\mathrm{dyn}})\cos(\theta_{\mathrm{dyn}}) - \theta_{\mathrm{dyn}}}$$

while the pressure field $p(r,\theta)$ is given by:

$$p(r,\theta) = \frac{\eta}{r}\frac{4V\cos(\theta)\sin(\theta_{\mathrm{dyn}})}{\sin(2\theta_{\mathrm{dyn}}) - 2\theta_{\mathrm{dyn}}}$$

where η is the dynamic viscosity. Here the free surface is located at $\theta = 0$ while the solid substrate is located at $\theta = -\theta_{\mathrm{dyn}}$. Note that this solution requires the presence of a normal surface pressure $4V\mu\sin(\theta_{\mathrm{dyn}})/(r(\sin(2\theta_{\mathrm{dyn}}) - 2\theta_{\mathrm{dyn}}))$ at the free surface in order to keep the interface flat. Using the solution above for the velocity and pressure fields, one can easily calculate the horizontal projection of the viscous force as:

$$\vec{e}_x \cdot \vec{f}_{\mathrm{s}} = -4V\eta\frac{\sin^2(\theta_{\mathrm{dyn}})}{\sin(2\theta_{\mathrm{dyn}}) - 2\theta_{\mathrm{dyn}}}$$

A striking feature of this result is that, although the pressure and stress fields diverge at the corner with a singularity in $\sim r^{-1}$, the resulting viscous force at the corner is finite and in fact independent of the choice of contour.

In addition to the viscous force, there is also a contribution at the tip of the moving wedge coming from the divergent surface pressure $4V\mu\sin(\theta_{\mathrm{dyn}})/(r(\sin(2\theta_{\mathrm{dyn}}) - 2\theta_{\mathrm{dyn}}))$ at the free surface needed to keep the interface flat. The usual approximation in dynamical wetting consists in integrating this contribution between a microscopic scale r_{min} and a macroscopic scale r_{max} in order to obtain the force $\vec{f_{\mathrm{ext}}}$, leading to:

$$\vec{e}_x \cdot \vec{f_{\mathrm{ext}}} = 4V\eta\frac{\sin^2(\theta_{\mathrm{dyn}})}{\sin(2\theta_{\mathrm{dyn}}) - 2\theta_{\mathrm{dyn}}}\ln\left(\frac{r_{\mathrm{max}}}{r_{\mathrm{min}}}\right)$$

Once lumped together with the viscous force at the tip by defining $r'_{max} = er_{max}$ with e the Euler constant, we obtain the following force balance at the tip of the moving wedge:

$$\cos(\theta_{\mathrm{dyn}}) - \cos(\theta_{\mathrm{eq}}) = 4\mathscr{C}_a\frac{\sin^2(\theta_{\mathrm{dyn}})}{\sin(2\theta_{\mathrm{dyn}}) - 2\theta_{\mathrm{dyn}}}\ln\left(\frac{r'_{\mathrm{max}}}{r_{\mathrm{min}}}\right)$$

where $\mathscr{C}_a = \eta V/\gamma_\ell$ is the capillary number. In the small-angle limit ($\theta_{\mathrm{eq}} \ll 1$, $\theta_{\mathrm{dyn}} \ll 1$), we recover the classical de Gennes model of wetting:

$$\theta_{\mathrm{dyn}}\left(\theta_{\mathrm{dyn}}^2 - \theta_{\mathrm{eq}}^2\right) = 6\mathscr{C}_a\ln\left(\frac{r'_{\mathrm{max}}}{r_{\mathrm{min}}}\right)$$

The De Gennes model makes the assumption that the interface remains flat in the vicinity of the contact line. This constraint must be enforced by hypothesizing the existence of an *ad-hoc* external force of unknown origin. The flat interface approximation can easily be relaxed by allowing the dynamic contact angle to vary over space, $\theta_{\mathrm{dyn}} = \theta_{\mathrm{dyn}}(r)$. In that case the divergent viscous stress is directly balanced by the Laplace pressure:

$$-\frac{4V\eta}{r}\frac{\sin(\theta_{\mathrm{dyn}})}{\sin(2\theta_{\mathrm{dyn}}) - 2\theta_{\mathrm{dyn}}} = \gamma_\ell\frac{\partial\theta_{\mathrm{dyn}}}{\partial r}$$

which can be rewritten after standard manipulation:

$$\mathscr{C}_a\ln\left(\frac{r}{r_{\mathrm{min}}}\right) = \int_{\theta_{\mathrm{dyn}}^{\mathrm{min}}}^{\theta_{\mathrm{dyn}}}\frac{\theta - \sin(\theta)\cos(\theta)}{2\sin\theta}\mathrm{d}\theta \qquad (62)$$

where we have introduced the microscopic contact angle $\theta_{\mathrm{dyn}}^{\mathrm{min}} = \theta_{\mathrm{dyn}}(r_{\mathrm{min}})$. Introducing the function $g(\theta)$:

$$g(\theta) = \int_0^\theta\frac{z - \sin z\cos z}{2\sin z}\mathrm{d}z,$$

Eq.(62) can be rewritten:

$$\mathscr{C}_a\ln\left(\frac{r}{r_{\mathrm{min}}}\right) = g(\theta_{\mathrm{dyn}}) - g(\theta_{\mathrm{dyn}}^{\mathrm{min}})$$

and we recognize immediately the Cox-Voinov relation[115,116].

4.2 Predictions for the general case

We now turn to the so far largely unexplored case of a viscous liquid moving over a viscoelastic substrate. In order to keep the model as simple as possible, we shall make the assumption that the viscous shear stress exerted by the viscous liquid on the viscoelastic substrate can be neglected and the sole force exerted by the liquid on the viscoelastic substrate is due to the (moving) capillary force at the contact line. Under this assumption, the microscopic contact angle is selected at small scales by the nonlinear force balance (50):

$$\begin{aligned} -\frac{\cos\theta_{\mathrm{dyn}}^{\mathrm{min}}}{\sin^2\theta_{\mathrm{dyn}}^{\mathrm{min}}} &= \frac{\gamma_\ell}{\gamma_{\mathrm{s}}}\left(\mathscr{F}_{cap}(H,V,\mu,\gamma_{\mathrm{s}}) + \mathscr{F}_{ve}(H,V,\mu,\gamma_{\mathrm{s}})\right) \\ &\equiv \mathscr{A} \end{aligned} \qquad (63)$$

where the explicit dependence of $\mathscr{A}$ on H, V, μ, γ_ℓ and γ_{s} has been omitted without ambiguity to lighten the notation. The solution of this transcendental equation is, under the condition

that $\theta_{\rm dyn}^{\rm min}=\pi/2$ at vanishing velocity:

$$\theta_{\rm dyn}^{\rm min}=\frac{\pi}{2}+\arctan\left(\frac{\sqrt{1+4\mathscr{A}^2}-1}{2}\right)^{\frac{1}{2}}$$

Plugging this result into the Cox-Voinov relation above, we obtain:

$$g(\theta_{\rm dyn})=\mathscr{C}_a\ln\left(\frac{r}{r_{\rm min}}\right)+g\left(\frac{\pi}{2}+\arctan\left(\frac{\sqrt{1+4\mathscr{A}^2}-1}{2}\right)^{\frac{1}{2}}\right)$$

In order to make further progress it is necessary to choose a rheological model for the viscoelastic substrate and, as previously, we will focus on the Chasset-Thirion rheology. With this choice, and recalling the definition of the dimensionless velocity $\Xi=V\tau/\overline{\ell_{\rm s}}$ and dimensionless thickness $\Lambda=H/\overline{\ell_{\rm s}}$, we obtain:

$$\begin{aligned} g(\theta_{\rm dyn}) &= g\left(\frac{\pi}{2}+\arctan\left(\frac{\sqrt{1+4\mathscr{A}^2(\mathscr{R}\mathscr{C}_a,\Lambda)}-1}{2}\right)^{\frac{1}{2}}\right) \\ &+\mathscr{C}_a\log\left(\frac{r}{r_{\rm min}}\right) \end{aligned} \tag{64}$$

Here we have defined the dimensionless number $\mathscr{R}$:

$$\mathscr{R}=\frac{2\mu\tau\gamma_\ell}{\eta\overline{\gamma_{\rm s}}}=\frac{\tau\gamma_{\ell{\rm v}}}{\bar{\ell}_{\rm s}\eta}$$

which is a measure of the relative influence of dissipation in the viscoelastic substrate and in the drop. This number can also be seen as the inverse of a capillary number for the motion of the liquid, where the velocity of the droplet is replaced by a characteristic velocity defined with respect to intrinsic properties of the solid substrate, $\mathscr{U}_{ve}=\bar{\ell}_{\rm s}/\tau$. At $\mathscr{R}=0$ dissipation occurs only in the viscous drop and we recover the Cox-Voinov law for an equilibrium angle of $\pi/2$:

$$g(\theta_{\rm dyn})=\mathscr{C}_a\ln\left(\frac{r}{r_{\rm min}}\right)+g(\pi/2)$$

The limit of large $\mathscr{R}$ is relevant to the case of a water drop moving on a soft viscoelastic substrate. In this situation, $\mathscr{R}\sim 6.10^4$. In Fig. 7 the dynamic contact angle $\theta_{\rm dyn}$ is plotted as a function of the capillary number $\mathscr{C}_a$ for several values of the number $\mathscr{R}$. The most striking feature of this model is that , as the dissipation in the substrate increases, *i.e.* when $\mathscr{R}$ increases, the $\theta_{\rm dyn}$-$\mathscr{C}_a$ curves exhibit an hysteresis-like behavior characterized by an abrupt change of the dynamic contact angle around $\mathscr{C}_a=0$ (Fig. 7A). However, the contact angle is never multi-valued within the present framework. Therefore, this apparent or soft hysteresis results from the high substrate dissipation. For high values of $\mathscr{R}$ and at small $\mathscr{C}_a$, the dynamic contact angle is selected by the nonlinear force balance (50) and thus independent of viscous dissipation in the drop (Fig. 7-B). When the capillary number $\mathscr{C}_a\sim 1/\mathscr{R}$ the dynamic contact angle reaches a plateau before increasing again as viscous dissipation becomes significant. As the capillary number further increases, the dynamic contact angle increases asymptotically to π. In view of the results of the previous section, it is easy to show that, in the limit $\mathscr{R}\to\infty$ the amplitude $\Delta\theta$ of this soft hysteresis is independent of the substrate thickness and given

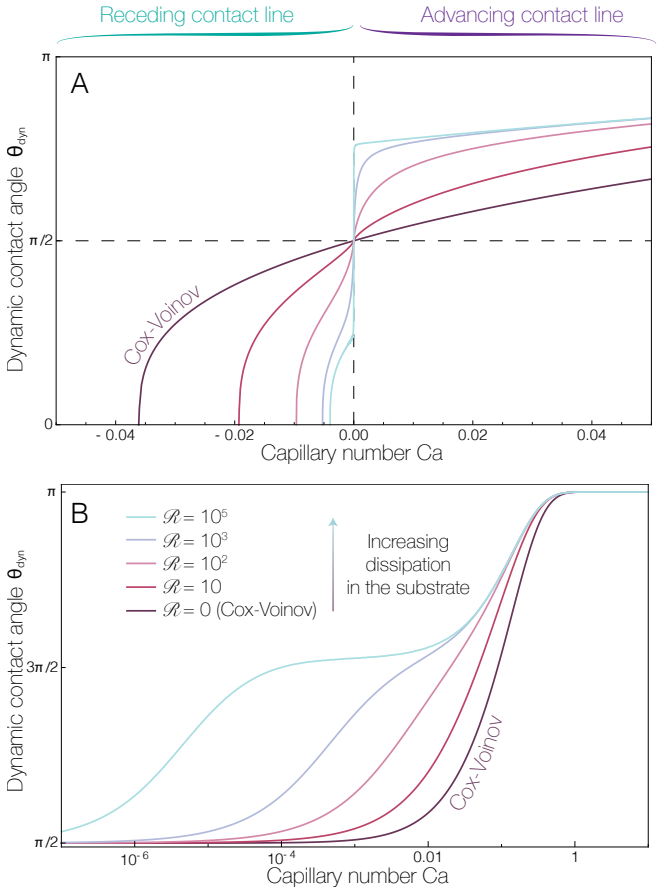

Fig. 7 Relation between the dynamic contact angle and the capillary number $\mathscr{C}_a$ for various values of the number $\mathscr{R}$. The values of $\mathscr{R}$ are given in panel (B) and apply to both panels. Other values of the physical parameters are as follow: $\Lambda=100$, $m=0.66$, $\gamma_\ell/2\overline{\gamma_{\rm s}}=0.8$. A: dynamic contact angle, in both the advancing and receding regimes. At $\mathscr{R}=0$ the energy is entirely dissipated in the liquid film and we recover the Cox-Voinov law. As $\mathscr{R}$ increases, an apparent hysteresis appears. For receding contact lines, there is also a strong decrease in the value of the critical capillary number at which the dynamic contact angle θ_{dyn} vanishes. B: details of the θ_{dyn}-$\mathscr{C}_a$ relationship for advancing contact lines in the apparent hysteresis region. The contact angle is never multivalued within the present framework but an apparent hysteresis occurs at large $\mathscr{R}$.

by:

$$\Delta\theta=2\pi-2\arctan\left(\frac{2}{\sqrt{1+4\left(\frac{\gamma_\ell}{\overline{\gamma_{\rm s}}}\frac{m}{1-m}\right)^2}-1}\right)^{\frac{1}{2}}$$

The second striking feature of the present model is observed for receding contact lines and is characterized by a marked decrease of the critical capillary number at which the dynamic contact angle vanish. This critical value controls the onset of deposition of Landau-Levich films. Interestingly, both a sharp change in dynamic contact angle at low capillary number, as well as a reduction in the critical capillary number for liquid film deposition were reported recently in wetting experiments on polymeric materials [117].

5 Discussion

We have shown in this paper that the generalized force balance (3) was able to describe accurately, and without any adjustable parameter, the dependence of the dynamic contact angle on

both the velocity of a contact line as well as the material and geometric properties of the soft substrate.

We have demonstrated that the motion of the triple line is opposed by both viscoelastic and capillary forces, the two contributions being equal in the limit of an infinitely thick substrate. This observation explains why, in a model based purely on capillarity, such as the Neuman force balance, the surface tension of the solid had to be redefined, by dividing it by ~ 2 in order to fit the experimental data[59]. Although this discrepancy was attributed to a finite slope effect, the model presented here shows that the reason for this disagreement comes from the absence of the viscoelastic force exerted by the substrate that resists contact line motion into the balance used to derive this value. Account for this force leads to a reasonable prediction. The success of our model also suggests that there is no need to invoke a rate dependence of the surface tension of the solid to explain data obtained in dynamics. Our mechanism is similar to the viscous relaxation observed in pendent drops of viscous liquids: the measurement of surface tension is accurate only when viscous relaxation is completed[118]. In a dynamic situation, such a relaxation hardly occurs and it should be accounted for in modeling attempts. Our model does so. In addition, we have also shown that the same equation allows to recover the classical de Gennes and Cox-Voinov models for the spreading of a viscous drop on a rigid substrate. Therefore, although the experimental data were limited to slowly moving drops, for which the dissipation mostly occurs in the viscoelastic substrate, we expect that the framework presented here will be able to describe much more general situations, for which dissipation occurs simultaneously in the solid and the liquid phases. In addition, the generalized force balance (3) can also be applied to the yet largely unexplored case of the spreading of a viscous drop over a viscous liquid bath.

6 Acknowledgments

We thank ANR (Agence Nationale de la Recherche) and CGI (Commisariat à l'Investissement d'Avenir) are gratefully acknowledged for their financial support through the GELWET project (ANR-17- CE30-0016), the Labex SEAM (Science and Engineering for Advanced Materials and devices - ANR 11 LABX 086, ANR 11 IDEX 05 02) and through the funding of the POLYWET and MMEMI projects.

Notes and references

1 Chandler D. Interfaces and the Driving Force of Hydrophobic Assembly. Nature. 2005 Sep;437(7059):640–7.

2 Berne BJ, Weeks JD, Zhou R. Dewetting and Hydrophobic Interaction in Physical and Biological Systems. Annu Rev Phys Chem. 2009 May;60(1):85–103.

3 de Gennes PG. Wetting: Statics and Dynamics. Rev Mod Phys. 1985 Jul;57(3):827–863.

4 De Gennes PG, Brochard-Wyart F, Quéré D. Capillarity and Wetting Phenomena - Drops, Bubbles, Pearls, Waves. 1st ed. New York: Springer-Verlag; 2004.

5 Rusanov AI. Surface Thermodynamics Revisited. Surf Sci Rep. 2005;58:111–239.

6 Bonn D, Eggers J, Indekeu J, Meunier J, Rolley E. Wetting and Spreading. Rev Mod Phys. 2009;81(2):739–805.

7 Maugis D. Contact, Adhesion and Rupture of Elastic Solids. vol. 130. Springer Science & Business Media; 2013.

8 Snoeijer JH, Andreotti B. Moving Contact Lines: Scales, Regimes, and Dynamical Transitions. Annu Rev Fluid Mech. 2013;45(1):269–292.

9 Liu T, Jagota A, Hui CY. A Closed Form Large Deformation Solution of Plate Bending with Surface Effects. Soft Matter. 2017 Jan;13(2):386–393.

10 Lawn B. Fracture of Brittle Solids. 2nd ed. Cambridge: Cambridge University Press; 1993.

11 Israelachvili JN. Intermolecular and Surface Forces. 3rd ed. Academic Press; 2011.

12 Gaisinskaya A, Ma L, Silbert G, Sorkin R, Tairy O, Goldberg R, et al. Hydration Lubrication: Exploring a New Paradigm. Faraday Discuss. 2012;156:217.

13 Rosen MJ. Surfactants and Interfacial Phenomena. 3rd ed. Wiley-Interscience; 2004.

14 Squires TM, Quake SR. Microfluidics: Fluid Physics at the Nanoliter Scale. Rev Mod Phys. 2005 Oct;77(3):977–1026.

15 Bixler GD, Bhushan B. Biofouling: Lessons from Nature. Philosophical Transactions of the Royal Society A: Mathematical, Physical and Engineering Sciences. 2012 May;370(1967):2381–2417.

16 Andrieu S, Müller P. Les Surfaces Solides: Concepts et Méthodes. EDP Sciences; 2012.

17 Feng J, Roché M, Vigolo D, Arnaudov LN, Stoyanov SD, Gurkov TD, et al. Nanoemulsions Obtained via Bubble-Bursting at a Compound Interface. Nat Phys. 2014;10(8):606–612.

18 Stoerzinger KA, Hong WT, Azimi G, Giordano L, Lee YL, Crumlin EJ, et al. Reactivity of Perovskites with Water: Role of Hydroxylation in Wetting and Implications for Oxygen Electrocatalysis. J Phys Chem C. 2015 Aug;119(32):18504–18512.

19 Han B, Stoerzinger KA, Tileli V, Gamalski AD, Stach EA, Shao-Horn Y. Nanoscale Structural Oscillations in Perovskite Oxides Induced by Oxygen Evolution. Nature Mater. 2017 Jan;16(1):121–126.

20 Labbé R, Duprat C. Capturing Aerosol Droplets with Fibers. Soft Matter. 2019 Sep;15(35):6946–6951.

21 Hills BA, Lichtenberger LM. Gastric Mucosal Barrier: Hydrophobicity of Stretched Stomach Lining. Am J Physiol-Gastrointest Liver Physiol. 1985;248:G643–G647.

22 Barthlott W, Neinhuis C. Purity of the Sacred Lotus, or Escape from Contamination in Biological Surfaces. Planta. 1997 Apr;202(1):1–8.

23 Chaudhury MK, Whitesides GM. How to Make Water Run Uphill. Science. 1992;256(5063):1539–1541.

24 Bertrand E, Bonn D, Broseta D, Dobbs H, Indekeu JO, Meunier J, et al. Wetting of Alkanes on Water. J Pet Sci Eng. 2002;33(1):217–222.

25 Shahidzadeh N, Bertrand E, Dauplait JP, Borgotti JC, Vié P, Bonn D. Effect of Wetting on Gravity Drainage in Porous Media. Transp Porous Media. 2003 Aug;52(2):213–227.

26 Sokuler M, Auernhammer GK, Roth M, Liu C, Bonacurrso E, Butt HJ. The Softer the Better: Fast Condensation on Soft Surfaces. Langmuir. 2010/02/02, 2010-02;26(3):1544–1547.

27 Wong TS, Kang SH, Tang SKY, Smythe EJ, Hatton BD, Grinthal A, et al. Bioinspired Self-Repairing Slippery Surfaces with Pressure-Stable Omniphobicity. Nature. 2011;477:443–447.
28 Ru C, Luo J, Xie S, Sun Y. A Review of Non-Contact Micro- and Nano-Printing Technologies. J Micromech Microeng. 2014;24:053001.
29 Delavoipière J, Heurtefeu B, Teisseire J, Chateauminois A, Tran Y, Fermigier M, et al. Swelling Dynamics of Surface-Attached Hydrogel Thin Films in Vapor Flows. Langmuir. 2018 Dec;34(50):15238–15244.
30 Young T. An Essay on the Cohesion of Fluids. Phil Trans R Soc Lond. 1805;95:65–87.
31 de Laplace PS. Traité de Mécanique Céleste; 1805. p. 67–78.
32 Dupré A. Théorie Mécanique de La Chaleur. Paris: Gauthier-Villars; 1869.
33 Butt HJ, Graf K, Kappl M. Physics and Chemistry of Interfaces. Weinheim: WILEY-VCH Verlag; 2003.
34 Bikerman JJ. Proc 2nd Intern Congr Surf Act. 1957;(III):125.
35 Bikerman JJ. Physical Surfaces. 1st ed. New York and London: Academic Press; 1970.
36 Lester GR. Contact Angles of Liquids at Deformable Solid Surfaces. J Colloid Sci. 1961;16(4):315–326.
37 Roman B, Bico J. Elasto-Capillarity: Deforming an Elastic Structure with a Liquid Droplet. J Phys Condens Matter. 2010 Nov;22(49):493101.
38 Andreotti B, Snoeijer JH. Soft Wetting and the Shuttleworth Effect, at the Crossroads between Thermodynamics and Mechanics. EPL Europhys Lett. 2016;113(6):66001.
39 Shanahan MER. The Spreading Dynamics of a Liquid Drop on a Viscoelastic Solid. J Phys D. 1988 Jun;21(6):981–985.
40 Carré A, Shanahan MER. Freinage Viscoélastique de l'étalement d'une Goutte. C R Acad Sci Paris. 1993;317(Série II):1153–1158.
41 Shanahan MER, Carré A. Anomalous Spreading of Liquid Drops on an Elastomeric Surface. Langmuir. 1994;10:1647–1649.
42 Carré A, Shanahan MER. Direct Evidence for Viscosity-Independent Spreading on a Soft Solid. Langmuir. 1995 Jan;11(1):24–26.
43 Shanahan MER, Carré A. Viscoelastic Dissipation in Wetting and Adhesion Phenomena. Langmuir. 1995;11:1396–1402.
44 Carré A, Gastel JC, Shanahan MER. Viscoelastic Effects in the Spreading of Liquids. Nature. 1996;379:432–434.
45 Carré A, Shanahan MER. Viscoelastic Braking of a Running Drop. Langmuir. 2001;17:2982–2985.
46 Shanahan MER, Carré A. Spreading and Dynamics of Liquid Drops Involving Nanometric Deformations on Soft Substrates. Colloid Surf A. 2002;206:115–123.
47 Long D, Ajdari A, Leibler L. Static and Dynamic Wetting Properties of Thin Rubber Films. Langmuir. 1996 Jan;12(21):5221–5230.
48 Long D, Ajdari A, Leibler L. How Do Grafted Polymer Layers Alter the Dynamics of Wetting ? Langmuir. 1996;12(6):1675–1680.
49 Mora S, Phou T, Fromental JM, Pismen L, Pomeau Y. Capillarity Driven Instability of a Soft Solid. Phys Rev Lett. 2010 Nov;105(21):1–4.
50 Mora S, Abkarian M, Tabuteau H, Pomeau Y. Surface Instability of Soft Solids under Strain. Soft Matter. 2011;.
51 Das S, Marchand A, Andreotti B, Snoeijer JH. Elastic Deformation Due to Tangential Capillary Forces. Phys Fluids. 2011;23(7):072006.
52 Jerison ER, Xu Y, Wilen LA, Dufresne ER. Deformation of an Elastic Substrate by a Three-Phase Contact Line. Phys Rev Lett. 2011 May;106(18):186103.
53 Marchand A, Das S, Snoeijer JH, Andreotti B. Contact Angles on a Soft Solid: From Young's Law to Neumann's Law. Phys Rev Lett. 2012 Dec;109(23):236101.
54 Marchand A, Das S, Snoeijer J, Andreotti B. Capillary Pressure and Contact Line Force on a Soft Solid. Phys Rev Lett. 2012 Feb;108(9):094301.
55 Mora S, Maurini C, Phou T, Fromental Jm, Audoly B, Pomeau Y. Solid Drops : Large Capillary Deformations of Immersed Elastic Rods. 2013;114301(September):1–5.
56 Paretkar D, Xu X, Hui CY, Jagota A. Flattening of a Patterned Compliant Solid by Surface Stress. Soft Matter. 2014 May;10(23):4084–4090.
57 Style RW, Wettlaufer JS, Dufresne ER. Surface Tension and the Mechanics of Liquid Inclusions in Compliant Solids. Soft Matter. 2014 Dec;11(4):672–679.
58 Mora S, Pomeau Y. Softening of Edges of Solids by Surface Tension. J Phys Condens Matter. 2015;27(19).
59 Karpitschka S, Das S, van Gorcum M, Perrin H, Andreotti B, Snoeijer JH. Droplets Move over Viscoelastic Substrates by Surfing a Ridge. Nat Commun. 2015;6:7891.
60 Zhao M, Dervaux J, Narita T, Lequeux F, Limat L, Roché M. Geometrical Control of Dissipation during the Spreading of Liquids on Soft Solids. Proc Nat Acad Sci USA. 2018;115:1748–1753.
61 Shanahan MER, de Gennes PG. L'arête Produite Par Un Coin Liquide Près de La Ligne Triple de Contact Solide/Liquide/Fluide. C R Acad Sci Paris. 1986;302:517–521.
62 Pericet-Camara R, Auernhammer GK, Koynov K, Lorenzoni S, Raiteri R, Bonaccurso E. Solid-Supported Thin Elastomer Films Deformed by Microdrops. Soft Matter. 2009;5(19):3611–3617.
63 Park SJ, Weon BM, Lee JS, Lee J, Kim J, Je JH. Visualization of Asymmetric Wetting Ridges on Soft Solids with X-Ray Microscopy. Nat Commun. 2014/07/10/online, 2014-07-10;5:4369 EP –.
64 Limat L. Straight Contact Lines on a Soft, Incompressible Solid. EPJ E. 2012;35:134–147.
65 Style RW, Dufresne ER. Static Wetting on Deformable Substrates, from Liquids to Soft Solids. Soft Matter. 2012;8(27):7177.
66 Style RW, Boltyanskiy R, Che Y, Wettlaufer JS, Wilen LA, Dufresne ER. Universal Deformation of Soft Substrates near a Contact Line and the Direct Measurement of Solid Surface Stresses. Phys Rev Lett. 2013 Feb;110(6):066103.
67 Bostwick JB, Shearer M, Daniels KE. Elastocapillary De-

formations on Partially-Wetting Substrates: Rival Contact-Line Models. Soft Matter. 2014;10(37):7361.

68 Lubbers LA, Weijs JH, Botto L, Das S, Andreotti B, Snoeijer JH. Drops on Soft Solids: Free Energy and Double Transition of Contact Angles. J Fluid Mech. 2014;747, R1:1–12.

69 Dervaux J, Limat L. Contact Lines on Soft Solids with Uniform Surface Tension : Analytical Solutions and Double Transition for Increasing Deformability. Proc R Soc A. 2015;471:20140813.

70 Style RW, Boltyanskiy R, Allen B, Jensen KE, Foote HP, Wettlaufer JS, et al. Stiffening Solids with Liquid Inclusions. Nature Phys. 2015 Jan;11(1):82–87.

71 Style RW, Boltyanskiy R, Che Y, Wettlaufer JS, Wilen LA, Dufresne ER. Universal Deformation of Soft Substrates near a Contact Line and the Direct Measurement of Solid Surface Stresses. Phys Rev Lett. 2013;(February):066103.

72 Shuttleworth R. The Surface Tension of Solids. Proc Roy Soc A. 1950;63:444–457.

73 Andreotti B, Bäumchen O, Boulogne F, Daniels KE, Dufresne ER, Perrin H, et al. Solid Capillarity: When and How Does Surface Tension Deform Soft Solids? Soft Matter. 2016;12(12):2993–2996.

74 Andreotti B, Snoeijer JH. Statics and Dynamics of Soft Wetting. Annu Rev Fluid Mech. 2020;52(1):null.

75 Xu Q, Jensen KE, Boltyanskiy R, Sarfati R, Style RW, Dufresne ER. Direct Measurement of Strain-Dependent Solid Surface Stress. Nat Commun. 2017;8(1):555.

76 Mondal S, Phukan M, Ghatak A. Estimation of Solid–Liquid Interfacial Tension Using Curved Surface of a Soft Solid. PNAS. 2015 Oct;112(41):12563–12568.

77 Schulman RD, Trejo M, Salez T, Raphaël E, Dalnoki-Veress K. Surface Energy of Strained Amorphous Solids. Nat Commun. 2018;9(1):982.

78 Tian Y, Ina M, Cao Z, Sheiko SS, Dobrynin AV. How To Measure Work of Adhesion and Surface Tension of Soft Polymeric Materials. Macromolecules. 2018 Jun;51(11):4059–4067.

79 Chen SY, Bardall A, Shearer M, E Daniels K. Distinguishing Deformation Mechanisms in Elastocapillary Experiments. Soft Matter. 2019;15(46):9426–9436.

80 Liang H, Cao Z, Wang Z, Dobrynin AV. Surface Stresses and a Force Balance at a Contact Line. Langmuir. 2018;34(25):7497–7502.

81 Liang H, Cao Z, Wang Z, Dobrynin AV. Surface Stress and Surface Tension in Polymeric Networks. ACS Macro Lett. 2018;7(1):116–121.

82 Masurel R, Roché M, Limat L, Ionescu I, Dervaux J. Elastocapillary Ridge as a Noninteger Disclination. Phys Rev Lett. 2019 Jun;122(24):248004.

83 Shafrin EG, Zisman WA. Upper Limits to the Contact Angles of Liquids on Solids. In: Fowkes FM, editor. Contact Angle, Wettability, and Adhesion. vol. 43 of Advances in Chemistry. WASHINGTON, D.C.: AMERICAN CHEMICAL SOCIETY; 1964. p. 145–157.

84 Shafrin EG. Appendix to Chapter 3 - Critical Surface Tensions of Polymers. In: Skeist I, editor. Handbook of Adhesives. 2nd ed. New York, N.Y., U.S.A.: Van Nostrand Reinhold Co.; 1977. p. 67–71.

85 Chaudhury MK, Whitesides GM. Direct Measurement of Interfacial Interactions between Semispherical Lenses and Flat Sheets of Poly(Dimethylsiloxane) and Their Chemical Derivatives. Langmuir. 1991 May;7(5):1013–1025.

86 Owen MJ, Dvornic PR. Silicone Surface Science. 1st ed. No. 4 in Advances in Silicon Science. New York: Springer; 2012.

87 McLoughlin K, Szeto C, Duncan TM, Cohen C. End-Linked Poly(Dimethylsiloxane) Elastomer Structure: ^{2} H-NMR Transverse Dephasing Data Compared to Predictions of Statistical and Thermodynamic Models. Macromolecules. 1996 Jan;29(16):5475–5483.

88 Lapinski N, Liu Z, Yang S, Hui CY, Jagota A. A Surface with Stress, Extensional Elasticity, and Bending Stiffness. Soft Matter. 2019 May;15(18):3817–3827.

89 Wu H, Liu Z, Jagota A, Hui CY. Effect of Large Deformation and Surface Stiffening on the Transmission of a Line Load on a Neo-Hookean Half Space. Soft Matter. 2018;14(10):1847–1855.

90 de Pascalis R, Dervaux J, Ionescu I, Limat L. Numerical Multiscale Modelling of Nonlinear Elastowetting. Eur J Mech - ASolids. 2018;71:151–164.

91 van Gorcum M, Karpitschka S, Andreotti B, Snoeijer J. Spreading on Viscoelastic Solids: Are Contact Angles Selected by Neumann's Law? Soft Matter. 2019 Dec;.

92 Eshelby JD. The Force on an Elastic Singularity. Philos Trans R Soc Lond Ser Math Phys Sci. 1951 Nov;244(877):87 LP – 112.

93 Mura T. The Elastic Field of Moving Dislocations and Disclinations(Green Function and Fourier Integrals in Dynamic Elastic Field Theory of Crystal Dislocations and Disclinations). Fundam Asp Dislocation Theory. 1970;2.

94 Eshelby JD. The force on a disclination in a liquid crystal. Philosophical Magazine A. 1980;42(3):359–367.

95 de Gennes PG, Prost J. The Physics of Liquid Crystals. 2nd ed. Oxford Science Publications, Oxford; 1995.

96 Peach M, Koehler JS. The Forces Exerted on Dislocations and the Stress Fields Produced by Them. Phys Rev. 1950 Nov;80(3):436–439.

97 Maugin GA. Material Inhomogeneities in Elasticity. Applied Mathematics. Taylor & Francis; 1993.

98 Maugin GA. Configurational Forces: Thermomechanics, Physics, Mathematics, and Numerics. Modern Mechanics and Mathematics. CRC Press; 2016.

99 Ogden RW. Non-Linear Elastic Deformations. Series in Mathematics and Its Applications. Ellis Horwood Ltd.; 1984.

100 Poisson SD. Memoire sur la theorie du Son. J Ecole Polytech Paris. 1808;7:319–392.

101 Rankine WJM. On the thermodynamic theory of waves of finite longitudinal disturbance. Philos Trans R Soc Lond. 1870;160:277–286.

102 Hugoniot PH. Memoire sur la propagation du mouvement dans les corps et plus specialement dans les gaz parfaits, Partie 1. J Ecole Polytech Paris. 1887;57:3–97.

103 Hugoniot PH. Memoire sur la propagation du mouvement dans les corps et plus specialement dans les gaz parfaits, Partie 2. J Ecole Polytech Paris. 1889;58:1–125.

104 Lamé G, Clapeyron BP. MÃľmoire sur la solidification par refroidissement d'un globe liquide. Ann Chimie Physique. 1831;47:250–256.

105 Stefan J. Ueber die Theorie der Eisbildung, insbesondere ueber die Eisbildung im Polarmeere. Ann Physik Chemie. 1891;42:269–286.

106 Nemat-Nasser S. Plasticity: A Treatise on Finite Deformation of Heterogeneous Inelastic Materials. Cambridge University Press; 2003.

107 Maugin GA, Trimarco C. Pseudomomentum and Material Forces in Nonlinear Elasticity: Variational Formulations and Application to Brittle Fracture. Acta Mech. 1992;94(1):1–28.

108 Henrot A, Pierre M. Variation et optimisation de formes: une analyse gÃľomÃľtrique. Springer; 2005.

109 Batra RC. The Force on a Lattice Defect in an Elastic Body. J Elast. 1987;17(1):3–8.

110 de Wit R. Theory of Disclinations: IV. Straight Disclinations. J Res Natl Bur Stand Phys Chem. 1973;77(5).

111 Malkov VM, Malkova YV. Investigation of the non-linear Flamant problem. Vestnik St Peterburg Univ Ser 1 Matematika Mekhanika Astronomiya. 2004;4:73–82.

112 Malkov VM, Malkova YV. Investigation of the non-linear Flamant problem. Izv Ross Akad Nauk MTT. 2006;5:68–78.

113 Curro JG, Pincus P. A Theoretical Basis for Viscoelastic Relaxation of Elastomers in the Long-Time Limit. Macromolecules. 1983;16(4):559–562.

114 Moffatt HK. Viscous and Resistive Eddies near a Sharp Corner. J Fluid Mech. 1964;18(1):1018.

115 Voinov OV. Hydrodynamics of Wetting. Fluid Dyn. 1976;11(5):714–721.

116 Cox RG. The Dynamics of the Spreading of Liquids on a Solid-Surface. Part 1. Viscous-Flow. J Fluid Mech. 1986;168:169–194.

117 Hayoun P. Partial wetting of thin liquid films in polymer tubes. Paris 6; 2016.

118 Jůza J. Surface Tension Measurements of Viscous Materials by Pendant Drop Method: Time Needed to Establish Equilibrium Shape. Macromol Symp. 2019;384(1):1800150.

Appendix A: Displacement field near the ridge tip

Let us first give the first-order solution of the boundary-value problem (30-34) for the displacement field $u_x^{(1)}, u_y^{(1)}$ and pressure field $p^{(1)}$ in the frame of the moving ridge $(x' = x - Vt, y)$:

$$u_x^{(1)}(x',y) = -\frac{1}{2\pi}\int_{-\infty}^{\infty} \frac{i\gamma_\ell e^{(y|k|+ikx')} y}{\gamma_s k + 2\mu[-kV]\mathrm{sign}(k)}\mathrm{d}k, \quad (65)$$

$$u_y^{(1)}(x',y) = -\frac{1}{2\pi}\int_{-\infty}^{\infty} \frac{\gamma_\ell e^{(y|k|+ikx')}(-1+y|k|)}{\gamma_s k^2 + 2\mu[-kV]|k|}\mathrm{d}k, \quad (66)$$

$$p^{(1)}(x',y) = -\frac{1}{2\pi}\int_{-\infty}^{\infty} \frac{2\gamma_\ell \mu[-kV] e^{(y|k|+ikx')}|k|}{\gamma_s k^2 + 2\mu[-kV]|k|}\mathrm{d}k, \quad (67)$$

Let us now introduce the polar coordinate system (r,θ) centered on the moving ridge tip. Close to the tip of the ridge (at $r \ll \ell_s$), the expressions above for the displacement field can be simplified. Working in the limit of vanishing velocity for simplicity, we find that for $r \ll \ell_s$:

$$u_x^{(1)}(r,\theta) = \frac{\gamma_\ell}{\mu}\left[\frac{\theta\cos(\theta)}{2\pi} + \frac{\sin(\theta)}{2\pi}\left(\gamma - 1 + \log\frac{r}{\ell_s}\right)\right]\frac{r}{\ell_s} + o(r\log r)$$

$$u_y^{(1)}(r,\theta) = -\frac{\gamma_\ell}{\mu}\left[\frac{\theta\sin(\theta)}{2\pi} - \frac{\cos(\theta)}{2\pi}\left(\gamma - 1 + \log\frac{r}{\ell_s}\right)\right]\frac{r}{\ell_s} + o(r\log r)$$

where $\gamma \approx 0.577$ is the Euler gamma constant and the o notation is the small o in Landau's notation. These expressions above are equivalent to the displacement field of a wedge disclination with Frank vector $2\gamma_\ell/\gamma_s$ [110]. It can also be seen directly from these expressions that they do not satisfy one of the compatibility equations of elasticity [110].

Appendix B: Derivation of the nonlinear force at the moving contact line

Using the contours defined in Fig. 8, the nonlinear force $\vec{f}_s$ can be expressed as:

$$\vec{f}_s = \lim_{\varepsilon\to 0}\int_{C_\varepsilon} \boldsymbol{\sigma}\cdot\vec{\nu}\ \mathrm{d}\ell$$

because the contour C_ε is now oriented in the anti-clockwise sense but the normal $\vec{\nu}$ is oriented toward the tip of the ridge. In order to calculate this force, let us consider the oriented compound contour $\mathscr{C}$ defined as $\mathscr{C} = C_1 \cup C_\varepsilon \cup C_2 \cup C_R$. This contour contain no singularity and thus, in absence of body force and acceleration, Cauchy theorem states that:

$$\int_{\mathscr{C}} \boldsymbol{\sigma}\cdot\vec{\nu}\mathrm{d}\ell = 0$$

which can be rewritten as:

$$\int_{C_R} \boldsymbol{\sigma}\cdot\vec{\nu}\mathrm{d}\ell + \int_{C_\varepsilon} \boldsymbol{\sigma}\cdot\vec{\nu}\mathrm{d}\ell + \int_{C_1\cup C_2} \boldsymbol{\sigma}\cdot\vec{\nu}\mathrm{d}\ell = 0$$

Since $\boldsymbol{\sigma}\cdot\vec{n} = \gamma_s\vec{n}\cdot(\nabla\vec{n})$ on $C_1 \cup C_2$, we have:

$$\int_{C_\varepsilon} \boldsymbol{\sigma}\cdot\vec{\nu}\mathrm{d}\ell = -\int_{C_R} \boldsymbol{\sigma}\cdot\vec{\nu}\mathrm{d}\ell - \int_{-R}^{-\varepsilon} \gamma_s\vec{n}\cdot(\nabla\vec{n})\mathrm{d}x - \int_{\varepsilon}^{R} \gamma_s\vec{n}\cdot(\nabla\vec{n})\mathrm{d}x \quad (68)$$

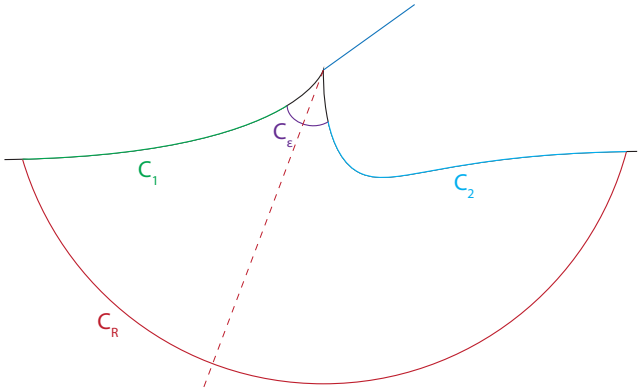

Fig. 8 Definition of the contours needed to obtain the nonlinear force at the ridge tip

In order to calculate the first integral appearing in the r.h.s. of equation (68) above, let us introduce the vector $\vec{v}_R$ as the radial unit vector in a frame attached at the tip of the ridge. We thus have:

$$\begin{aligned}\int_{C_R} \boldsymbol{\sigma}\cdot\vec{v}_R \mathrm{d}\ell &= \frac{\gamma_\ell}{2\gamma_s}\int_{C_R}\boldsymbol{\sigma}^{(1)}\cdot\vec{v}_R\mathrm{d}\ell \\ &+\left(\frac{\gamma_\ell}{2\gamma_s}\right)^2\int_{C_R}\left\{\boldsymbol{\sigma}^{(2)}+(\vec{u}^{(1)}\cdot\nabla)\boldsymbol{\sigma}^{(1)}\right\}\cdot\vec{v}_R\mathrm{d}\ell \\ &+\mathscr{O}\left(\frac{\gamma_\ell}{2\gamma_s}\right)^3 \end{aligned} \tag{69}$$

Now these two integrals can easily be calculated in the limit where the radius of the long arc C_R goes to infinity. In that case the first integral is simply equal to the vertical first order-force (i.e $\gamma_\ell \sin\theta_{\mathrm{dyn}}\vec{e}_y$) while the second-order term is given by the spatial integration of the boundary condition (40a), keeping in mind the orientation of the contour:

$$\begin{aligned}\lim_{R\to\infty}\int_{C_R}\boldsymbol{\sigma}\cdot\vec{v}_R\mathrm{d}\ell &= \gamma_\ell\sin(\theta_{\mathrm{dyn}})\vec{e}_y \\ &-\int_{-\infty}^{0^-}\gamma_s\vec{n}\cdot(\nabla\vec{n})\mathrm{d}x-\int_{0^+}^{\infty}\gamma_s\vec{n}\cdot(\nabla\vec{n})\mathrm{d}x \\ &+\vec{e}_x\left\{\int_{-\infty}^{0^-}\sigma_{xx}^{(1)}\frac{\partial\zeta^{(1)}}{\partial x}\,\mathrm{d}x+\int_{0^+}^{\infty}\sigma_{xx}^{(1)}\frac{\partial\zeta^{(1)}}{\partial x}\,\mathrm{d}x\right\}\end{aligned} \tag{70}$$

Now we plug the result above in equation (68) and multiply the result by $\vec{e}_x$ in order to obtain, upon taking both the limit $R\to\infty$ and $\varepsilon\to 0$:

$$\vec{e}_x\cdot\vec{f}_s=\left(\frac{\gamma_\ell}{2\gamma_s}\right)^2\left\{\int_{-\infty}^{0^-}\sigma_{xx}^{(1)}\frac{\partial\zeta^{(1)}}{\partial x}\,\mathrm{d}x+\int_{0^+}^{\infty}\sigma_{xx}^{(1)}\frac{\partial\zeta^{(1)}}{\partial x}\,\mathrm{d}x\right\}+\mathscr{O}\left(\frac{\gamma_\ell}{2\gamma_s}\right)^3$$

Because the singularity of the integrand in the formula above is integrable, it can be rewritten, up to second-order, as:

$$\vec{e}_x\cdot\vec{f}_s=\left(\frac{\gamma_\ell}{2\gamma_s}\right)^2\int_{-\infty}^{\infty}\sigma_{xx}^{(1)}\frac{\partial\zeta^{(1)}}{\partial x}\,\mathrm{d}x$$